정지궤도 해양탑재체(GOCI)의 광학성능 수치모사 연구

Optical Performance Simulation of Geostationary Ocean Color Imager

2014. 12

한국해양과학기술원

제 출 문

한국해양과학기술원장 귀하

본 보고서를 “정지궤도 해양탑재체(GOCI)의 광학성능 수치모사 연구” 사업의 최종보고서로 제출합니다.

2015 . 2 . 28 .

총괄연구책임자 : 오 은 송

참 여 연 구 원 : 문 정 언

“ : 안 기 범

“ : 강 혁 모

요 약 문

Ⅰ. 제 목

○ 정지궤도 해양탑재체(GOCI)의 광학성능 수치모사 연구

Ⅱ. 연구개발의 목적 및 필요성

1. 기술적 측면

○ 해양과학기술원은 2010년 6월에 세계 최초의 정지궤도 해양관측위성인 GOCI(Geostationary Ocean Color Imager)를 성공적으로 개발, 발사, 운영을 하고 있음

○ 2010년 이후 GOCI는 한반도를 중심으로 동북아시아 해역의 해양기후변화 및 해양환경변화에 대한 모니터링을 수행하고 있으며, 재난/재해 등 각종 현안 대응에도 힘쓰고 있음

○ 이러한 각종 과학적 목적을 이루기 위해서는 GOCI 탑재체의 광학적 성능 추이를 정확히 파악하는 일이 필수적이며, 특히 초단기, 중장기적 센서의 변화를 측정하기 위해서는 성능 수치모사 시스템이 필요함

○ 정지궤도 위성이라는 특성상 태양-지구-위성 간 상호 작용에 대한 연구가 필요하며, 전 우주적인 관점에서 영상 성능에 대한 수치모사 연구가 필수적임

○ 광학계의 기기적인 특성 분석 및 영상처리 기법에 대한 연구는 탑재체로부터 도출되는 위성 영상의 품질에 직접적으로 영향을 미치기에 수치모사를 통해 검증되어야 함

○ 전 우주적인 수치모사 시스템을 포함한 광학성능 수치모사 연구는 GOCI 뿐만 아니라 연안/해양 원격탐사 연구에서 정량적인 복사휘도 값 및 반사도 등을 예측할 수 있어 유용하게 쓰일 것으로 예상됨

○ 또한, 현재 GOCI의 후속 위성인 GOCI-II 개발에 있어서도 실제 제작 전 탑재체 설계안에 대한 상세 분석을 통해, 과학적 임무 수행의 성과 예측 및 센서의 성능 예측 등을 수행할 수 있어, 개발 기간과 예산 절감의 효과는 물론 GOCI에 이어 지속적인 해양 관측 임무 수행에 큰 역할을 할 것임

2. 경제・산업적 측면

○ GOCI의 End-to-End 수치모사를 통하여 한반도 주변 해양 관측에 대한 각 종 예측하기 힘든 변화에 대한 수치적인 예측이 가능함. 이를 이용하여 해양환경의 광학적, 정량적 분석이 가능하고, 나아가 적조/녹조 와 같이 해수 반사도가 다르게 나타나는 해양 재난/재해에 대한 모델링을 개발이 가능하여 국내 어장 예측 정보에도 활용 가능함

○ 원격탐사 연구 측면에서, 본 과제에서 추진하고자 하는 기술개발은 위성 영상 수치모사의 연구 분야에서 국제적으로 유수의 연구자와 기관과의 협력 연구를 할 수 있는 매우 독창적이고 활용도가 높은 기술이라 할 수 있음

3. 사회・문화적 측면

○ 국내의 경제적 발전 동향과 맥을 같이 하는 과학기술 역량에 대한 국민적 자부심과 기대감이라는 사회문화적 배경 위에 GOCI 탑재체가 세계 최초의 정지궤도 해색센서로서 사용되어 해양관측

임무를 수행함에 있어, 그 과학적 결과의 정확성을 높일 수 있는 본 과제의 기술을 통해 사회적으로 안정적인 해양 자료를 제공 받을 수 있고, 세계 최초라는 국민적 자긍심을 높일 수 있는 효과가 매우 크다고 할 수 있음

○ 사회적으로 기후변화, 특히 전 지구의 70% 이상을 차지하고 있는 해양기후변화에 대한 관심이 크게 높아지고 있음. 이에 미래에 개발될 GOCI-II에도 본 기술이 적용됨으로써, 일반인들이 보다 객관적이고 정확한 관점에서 기후변화의 실상을 파악할 수 있으며, 사회적인 측면에서 볼 때 객관적이고 효율적인 해양기후변화 대응능력을 제고 할 수 있음

Ⅲ. 연구개발의 내용 및 범위

1. 연구기간

(1차년도) 2013년 1월 1일 ~ 2013년 12월 31일

(2차년도) 2014년 1월 1일 ~ 2014년 12월 31일

2. 연구개발의 내용 및 범위

구 분	목 표	내용 및 범위
1 차년도 (2013)	광선 추적 기법을 이용한 정지궤도 해양관측위성의 궤도상 잡광 분석 기술 개발	○GOCI에 대한 광선 추적 기반의 광학 성능 평가 시스템 구축의 선행연구 – 태양 모델을 통한 광원 설정 – 한반도 주변 설정 후 육지, 해양 반사율 및 산란 모델 적용 – GOCI 광학 시스템 내부의 산란 모델 적용 및 검출기 특성 부여 – 실제와 동일한 스케일을 통한 검출기에서의 영상과 복사량 측정 ○이미지 기반 성능평가 – 광선 추적 기법과 지향 반사경의 운용 시스템을 적용 – 슬롯 별 광선 추적 후 영상 처리 적용 – 슬롯 별 광원 모델과 특정한 주변 영향에 대한 영상 수치모사 ○GOCI를 통한 원격탐사 용 수치모사 시스템 선행연구 – 한반도 해역에 대한 지구모델과 GOCI의 실 운용 시스템을 접목 시킨 원격탐사 형태의 수치모사 수행 – Monte-Carlo 방식을 이용한 통계적 수치모사 수행 ○궤도상 GOCI 광학 시스템 내 잡광 분석 – GOCI 시스템 내부 산란 특성 분석 – 잡광 요인 분석 및 정량적인 잡광과 Ghost 량 추이 분석 – Step & Stare 방식에서의 주변 슬롯에 의한 잡광 분석 – 잡광 분석을 통한 영상에서의 잡광 분포를 통한 영상 재조합 수행

구 분	목 표	내용 및 범위
2 차년도 (2014)	정지궤도 해양탑재체(GOCI)의 광학 성능 수치모사 기법의 고도화	○통합적 광선추적 기법을 이용한 광학 복사 능력 검증 - GOCI의 궤도상 잡광 분석 - 광학 시스템 틀어짐에 따른 잡광 형태 변형 및 정량적 분석 - 통합적 광선추적 기법의 성능 검증 ○광학계 정렬 기법 수치모사를 통한 시스템 성능 검증 - 다중 설계 최적화 방법을 이용한 GOCI의 광학계 정렬 해 분석 - GOCI-II 광학계의 최적 정렬 방법 연구 - 정렬 기법 구현 프로그램 구축 ○영상처리 수치모사를 이용한 영상 품질 향상 - Wiener 필터를 이용한 MTF 보상 기법 연구 - MTF 보상 결과와 해양 산출물의 정확도 상관관계 연구 ○BRDF 측정 시스템 개발을 통한 수치모사 정확도 향상 - 해수 BRDF 측정 시스템 설계 및 구축 - 적분구의 불확도 측정 시험 - 해양 관측 장비의 수중 스펙트럼 수치모사

Ⅳ. 연구개발결과

1. 1차년도 연구수행 결과

○ 광선추적 기반 GOCI 광학 성능 분석 시스템 개발 선행연구
- 태양 모델을 통한 광원 설정 (Lambertian Scatter model + 태양광량 변화 고려)
- 한반도 주변 설정 후 육지, 해양 반사율 및 산란 모델 적용
- GOCI 광학 시스템 내부의 산란 모델 적용 및 검출기 특성 부여
- 실제와 동일한 스케일을 통해 검출기에서의 영상과 복사량 측정

○ 이미지 기반 성능평가
- 광선 추적 기법과 지향 반사경의 운용 시스템을 적용
- 슬롯 별 광선 추적 후 영상 처리 적용 (실제 촬영 영상과 상세 비교)
- 슬롯 별 광원 모델과 특정한 주변 영향에 대한 영상 수치모사

○ GOCI를 통한 원격탐사 용 수치모사 시스템 선행연구
- 해색의 적조 등 산란 모델을 적용한 지구모델 구현 (한반도 상세 모델 구현 초기 연구)
- 한반도 해역에 대한 지구모델과 GOCI의 실 운용 시스템을 접목 시킨 원격탐사 형태의 수치모사 수행
- Monte-Carlo 방식을 이용한 통계적 수치모사 수행 (대기 모델, 해양 모델 접목)

○ 궤도상 GOCI 광학 시스템 내 잡광 분석 (신진연구자 사업 주요 핵심 내용)
- GOCI 시스템 내부 산란 특성 분석
- 잡광 요인 분석 및 정량적인 잡광과 Ghost 량 추이 분석
- Step & Stare 방식에서의 주변 슬롯에 의한 잡광 분석

- 잡광 분석을 통한 영상에서의 잡광 분포를 통한 영상 재조합 수행

2. 2차년도 연구수행 결과

○ 통합적 광선추적 기법을 이용한 광학 복사 능력 검증
- 태양 모델을 통한 광원 설정 (Lambertian Scatter model + 태양광량 변화 고려)
- 한반도 주변 설정 후 육지, 해양 반사율 및 산란 모델 적용
- GOCI 광학 시스템 내부의 산란 모델 적용 및 검출기 특성 부여
- 실제와 동일한 스케일을 통해 검출기에서의 영상과 복사량 측정

○ 광학계 정렬 기법 수치모사를 통한 시스템 성능 검증
- GOCI 및 GOCI-II와 동일한 광학계 형태(TMA, Korsch 형태)에 대한 수치모사 수행
- CAA(Computer Aided Alignment) 기법의 연구 및 수치모사 수행
- GOCI의 Filter의 정렬 상태의 민감도 분석 수행을 통한 영상의 품질과의 연관성 분석
- 민감도 분석 방법 및 다중 구성 최적화 방법에 대한 정렬 S/W 구현 선행연구

○ 영상처리 수치모사를 이용한 영상 품질 향상
- GOCI에 최적화할 수 있는 Wiener Filter 설계
- 고해상도 영상을 이용하고, GOCI와 비교 검증을 통해 MTF 보상 기법 연구
- MTF 보상 결과와 해양 산출물의 정확도 상관관계 연구

○ BRDF 측정 시스템 개발을 통한 수치모사 정확도 향상
- 해수 표면의 BRDF 측정 시스템 개발
  a. 광학 실험실 내 표준광원 및 스펙트로미터 이용
  b. 고니어미터 형태의 다변각 BRDF 측정 수행
  c. 해수 생물학적 특성 변화에 따른 BRDF 변화 추이 분석
- 현장관측 용 BRDF 측정 기기 Prototype 개발
  a. 소규모 BRDF 측정 기기 개발
  b. 이동 가능한 형태의 측정 기기 설계/개발

Ⅴ. 연구개발결과의 활용계획

○ 현재 운용 중인 GOCI의 궤도상 성능 검증을 함으로써 해양 관측 임무 수행에 안정적인 자료 제공

○ 궤도상 잡광 분석을 전우주적 관점에서 수행하는 세계 최초의 연구를 수행하므로 써 정지궤도뿐만 아니라 저궤도, 항공용 탑재체의 운용 중 궤도상 잡광의 영향을 파악할 수 있는 기술을 개발

○ 차세대 해양관측 위성의 초기 개념 설계부터 광기계부 설계에 이르기 까지 End-to-end 수치모사 시스템을 구축하므로 써 시간과 개발 비용을 절약할 수 있으며, 월등한 요구사항을 지니는 차세대 해양관측 위성의 안정적인 개발을 가능하게 함

○ 본 연구 결과로 얻게 될 광선 추적 기반 정지궤도 해양탑재체 수치모사 시스템은 곧바로 현재 GOCI 활용 연구에 직접적으로 사용될 수 있으며, 추후 GOCI-II 개발에 있어서 성능 평가 및 향상에 기여하므로 써, 국내 우주개발 산업의 기술력을 배가시킬 것으로 예상됨

목 차

제 1 장 서 론

제 1 절 연구개발의 목적 및 필요성

가. 기술적 측면

○ 해양과학기술원은 2010년 6월에 세계 최초의 정지궤도 해양관측위성인 GOCI(Geostationary Ocean Color Imager)를 성공적으로 개발, 발사, 운영을 하고 있음

○ 2010년 이후 GOCI는 한반도를 중심으로 동북아시아 해역의 해양기후변화 및 해양환경변화에 대한 모니터링을 수행하고 있으며, 재난/재해 등 각종 현안 대응에도 힘쓰고 있음

○ 이러한 각종 과학적 목적을 이루기 위해서는 GOCI 탑재체의 광학적 성능 추이를 정확히 파악하는 일이 필수적이며, 특히 초단기, 중장기적 센서의 변화를 측정하기 위해서는 성능 수치모사 시스템이 필요함

○ 정지궤도 위성이라는 특성상 태양-지구-위성 간 상호 작용에 대한 연구가 필요하며, 전 우주적인 관점에서 영상 성능에 대한 수치모사 연구가 필수적임

○ GOCI 뿐만 아니라 전 우주적인 수치모사 시스템은 연안/해양 원격탐사 연구에서 정량적인 복사휘도 값 및 반사도 등을 예측할 수 있어 유용하게 쓰일 것으로 예상됨

○ 또한, 현재 GOCI의 후속 위성인 GOCI-II 개발에 있어서도 실제 제작 전 탑재체 설계안에 대한 상세 분석을 통해, 과학적 임무 수행의 성과 예측 및 센서의 성능 예측 등을 수행할 수 있어, 개발 기간과 예산 절감의 효과는 물론 GOCI에 이어 지속적인 해양 관측 임무 수행에 큰 역할을 할 것임

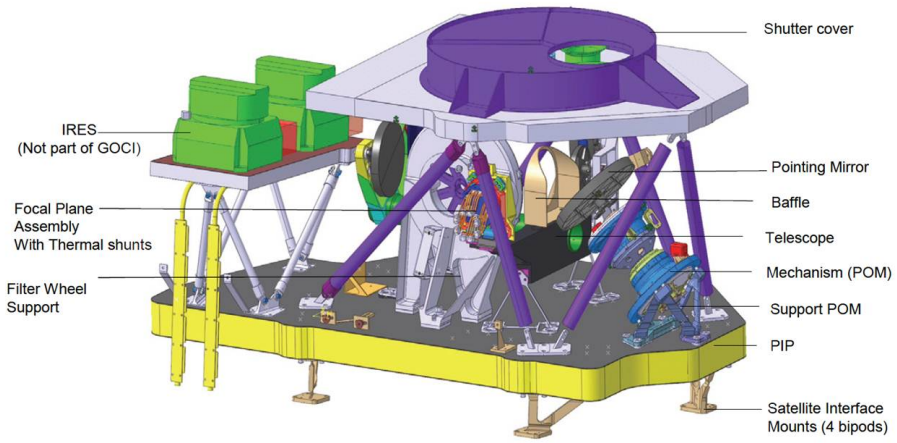

나. 경제, 산업적 측면

○ GOCI의 End-to-End 수치모사를 통하여 한반도 주변 해양 관측에 대한 각 종 예측하기 힘든 변화에 대한 수치적인 예측이 가능함. 이를 이용하여 해양환경의 광학적, 정량적 분석이 가능하고, 나아가 적조/녹조 와 같이 해수 반사도가 다르게 나타나는 해양 재난/재해에 대한 모델링을 개발이 가능하여 국내 어장 예측 정보에도 활용 가능함
○ 원격탐사 연구 측면에서, 본 과제에서 추진하고자 하는 기술개발은 위성 영상 수치모사의 연구 분야에서 국제적으로 유수의 연구자와 기관과의 협력 연구를 할 수 있는 매우 독창적이고 활용도가 높은 기술이라 할 수 있음

다. 사회, 문화적 측면

○ 국내의 경제적 발전 동향과 맥을 같이 하는 과학기술 역량에 대한 국민적 자부심과 기대감이라는 사회문화적 배경 위에 GOCI 탑재체가 세계 최초의 정지궤도 해색센서로서 사용되어 해양관측 임무를 수행함에 있어, 그 과학적 결과의 정확성을 높일 수 있는 본 과제의 기술을 통해 사회적으로 안정적인 해양 자료를 제공 받을 수 있고, 세계 최초라는 국민적 자긍심을 높일 수 있는 효과가 매우 크다고 할 수 있음
○ 사회적으로 기후변화, 특히 전 지구의 70% 이상을 차지하고 있는 해양기후변화에 대한 관심이 크게 높아지고 있음. 이에 미래에 개발될 GOCI-II에도 본 기술이 적용됨으로써, 일반인들이 보다 객관적이고 정확한 관점에서 기후변화의 실상을 파악할 수 있으며, 사회적인 측면에서 볼 때 객관적이고 효율적인 해양기후변화 대응능력을 제고 할 수 있음

제 2 절 연구개발의 범위

본 연구에서는 정지궤도 해양탑재체(GOCI)의 광학성능 수치모사 연구를 다음과 같이 수행하였음

구 분	목 표	내용 및 범위
1 차년도 (2013)	광선 추적 기법을 이용한 정지궤도 해양관측위성의 궤도상 잡광 분석 기술 개발	○GOCI에 대한 광선 추적 기반의 광학 성능 평가 시스템 구축의 선행연구 - 태양 모델을 통한 광원 설정 - 한반도 주변 설정 후 육지, 해양 반사율 및 산란 모델 적용 - GOCI 광학 시스템 내부의 산란 모델 적용 및 검출기 특성 부여 - 실제와 동일한 스케일을 통한 검출기에서의 영상과 복사량 측정 ○이미지 기반 성능평가 - 광선 추적 기법과 지향 반사경의 운용 시스템을 적용 - 슬롯 별 광선 추적 후 영상 처리 적용 - 슬롯 별 광원 모델과 특정한 주변 영향에 대한 영상 수치모사 ○GOCI를 통한 원격탐사 용 수치모사 시스템 선행연구 - 한반도 해역에 대한 지구모델과 GOCI의 실 운용 시스템을 접목 시킨 원격탐사 형태의 수치모사 수행 - Monte-Carlo 방식을 이용한 통계적 수치모사 수행 ○궤도상 GOCI 광학 시스템 내 잡광 분석 - GOCI 시스템 내부 산란 특성 분석 - 잡광 요인 분석 및 정량적인 잡광과 Ghost 량 추이 분석 - Step & Stare 방식에서의 주변 슬롯에 의한 잡광 분석 - 잡광 분석을 통한 영상에서의 잡광 분포를 통한 영상 재조합 수행

구 분	목 표	내용 및 범위
2 차년도 (2014)	정지궤도 해양탑재체(GOCI)의 광학 성능 수치모사 기법의 고도화	○통합적 광선추적 기법을 이용한 광학 복사 능력 검증 - GOCI의 궤도상 잡광 분석 - 광학 시스템 틀어짐에 따른 잡광 형태 변형 및 정량적 분석 - 통합적 광선추적 기법의 성능 검증 ○광학계 정렬 기법 수치모사를 통한 시스템 성능 검증 - 다중 설계 최적화 방법을 이용한 GOCI의 광학계 정렬 해분석 - GOCI-II 광학계의 최적 정렬 방법 연구 - 정렬 기법 구현 프로그램 구축 ○영상처리 수치모사를 이용한 영상 품질 향상 - Wiener 필터를 이용한 MTF 보상 기법 연구 - MTF 보상 결과와 해양 산출물의 정확도 상관관계 연구 ○BRDF 측정 시스템 개발을 통한 수치모사 정확도 향상 - 해수 BRDF 측정 시스템 설계 및 구축 - 적분구의 불확도 측정 시험 - 해양 관측 장비의 수중 스펙트럼 수치모사

제 2 장 국내외 기술개발 현황

1. 국외 기술 현황

○ 지구관측 위성 중 하나인 Sentinel-2 위성의 경우, end-to-end 수치모사 기법을 통해 센서 관측 대역을 최적화 하고, 이에 알맞은 활용 연구를 추진하므로써, 위성을 체계적으로 개발하는데 활용되었음 (Segl. K., et al 2010)

○ 대기층의 산란 모델 등 정량적인 복사휘도, 조도 값을 연구하는 그룹의 경우 End-to-end 수치모사 기법을 통해 그 오차 값들을 추정하는 연구를 활발히 진행하고 있음 (Pougatchev, N., 2008)

○ GOCI와 유사한 임무를 띄고 운용중인 저궤도 해양관측위성 MODIS의 경우 광학 성능 수치모사를 통해 수많은 검보정 작업을 수행하고 있으며, MTF, SNR과 같은 주요 광학 성능의 추이를 파악하고자 수치모사 연구를 진행하고 있음

○ 해색위성에 대한 연구에서도 광원인 태양부터, 대기층의 복사 전달 모델, 해수 표면 및 해수 중의 복사 모델을 아우르는 통합적 수치모사 연구가 이뤄지고 있으며, 일련의 과정과 더불어 위성 센서의 광학적 성능까지 고려되는 수치모델이 개발 되고 있음

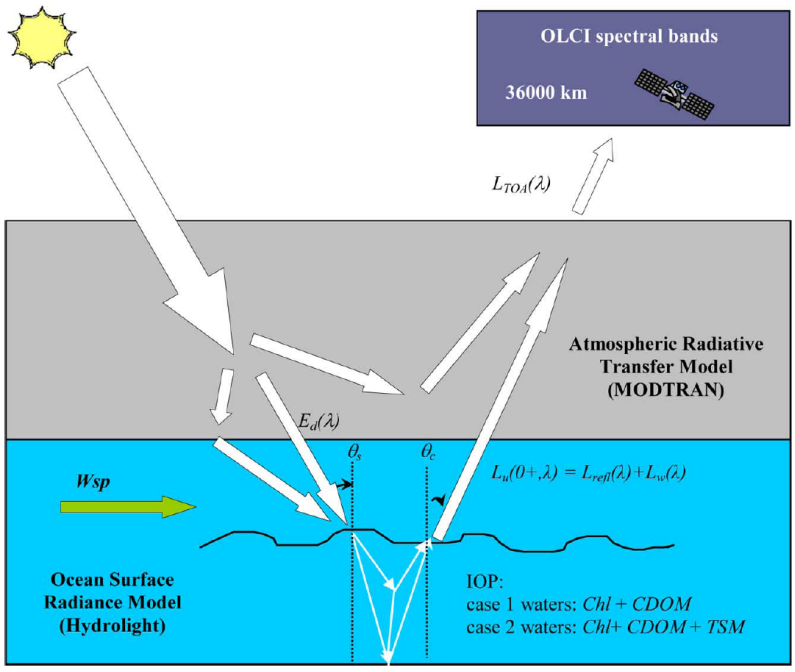

그림 1. 해양 위성 OLCI의 광학적 end-to-end 수치모사 개념도

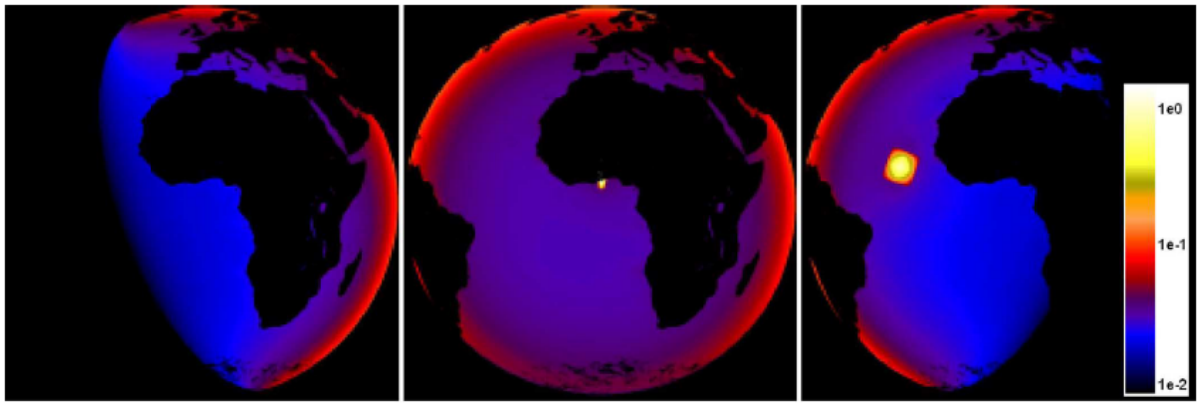

그림 2. 시간에 따른 TOA(Top of Atmosphere)에서의 복사량 수치모사

2. 국내 기술 현황

○ 광선추적기법을 이용한 육지, 해양, 대기, 식생분포 BSDF 등 지구 모델을 개발 하여 심우주 망원경의 성능 평가 및 분광 스펙트럼 결과 분석을 하는 연구가 활발히 진행되고 있음

○ End-to-End 성능 평가는 국방용 EO/IR 카메라 및 심우주 망원경, 지구 온난화 측정용 우주 망원경 등에 활용되고 있음

○ 저궤도 위성의 잡광 분석 용도로 활용되면서, 실제 설계 단계부터 조립 단계까지 그 성능 파악이 용이하다는 장점으로 국내외 연구소 및 개발 업체에서 다양하게 쓰이고 있음

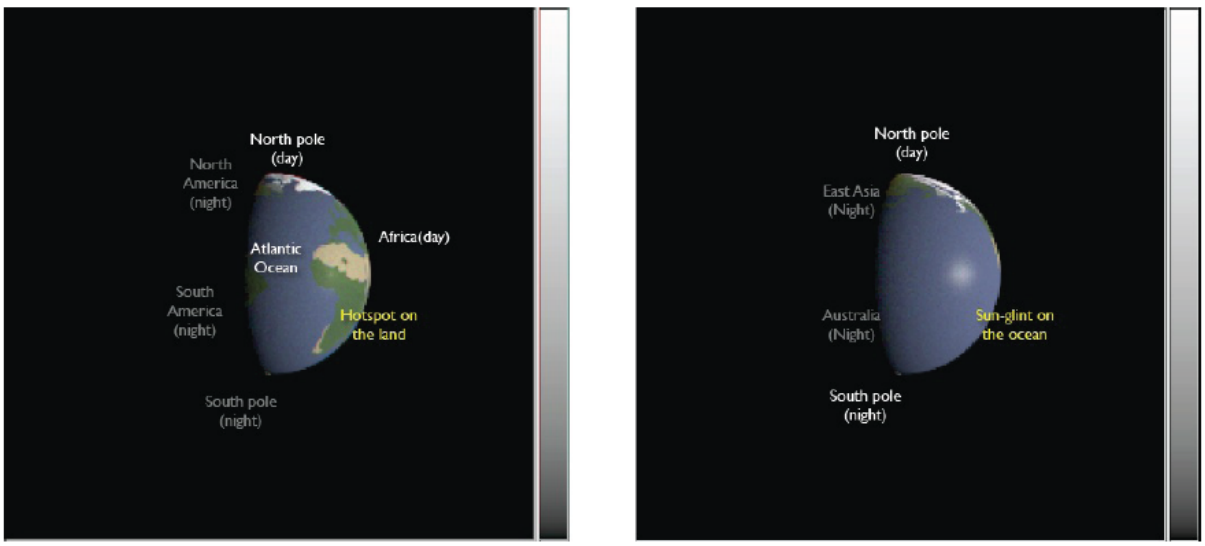

그림 3. 지구관측용 위성 광학계로 바라본 지구 모형 수치모사 (Ryu et al. 2012)

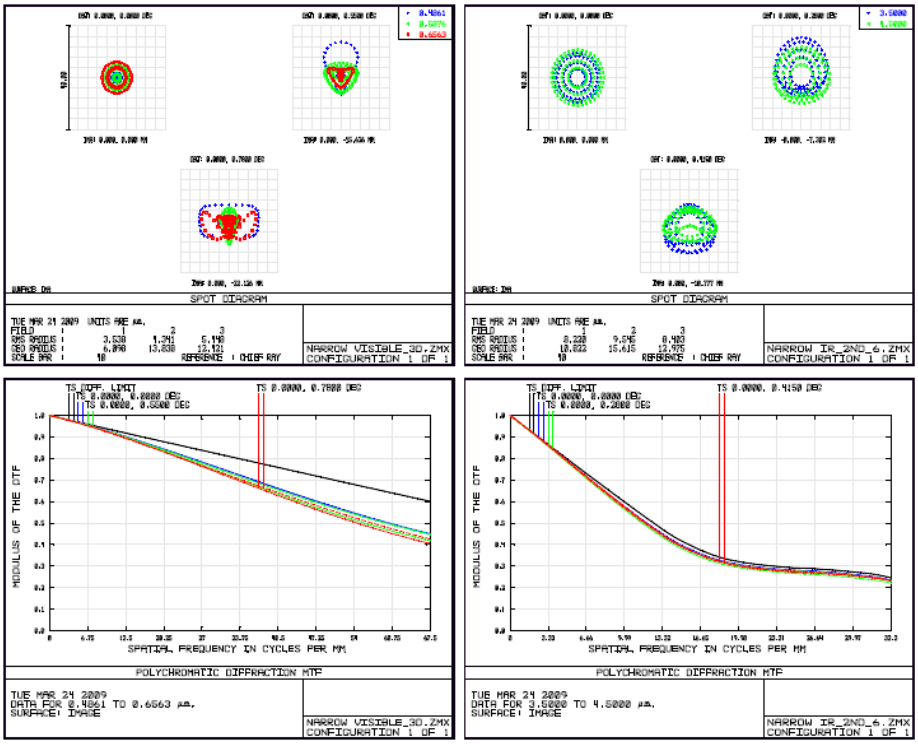

그림 4. 국방용 EO/IR 광학계의 성능 평가 (Seong et al. 2009)

제 3 장 연구개발 수행내용 및 결과

제 1 절 1차년도 연구개발 수행 내용

1. 통합적 광선 추적 수치모사기법(IRT, Integrated Ray Tracing) 개발

- (정의) 광원, 관측대상, 관측기기가 하나의 수치모사 환경에서 실제 크기로 구현되어 광선 추적의 방법을 통해 관측기기의 검출면에 도달하는 복사량과 결상 능력을 동시에 계산할 수 있는 기법

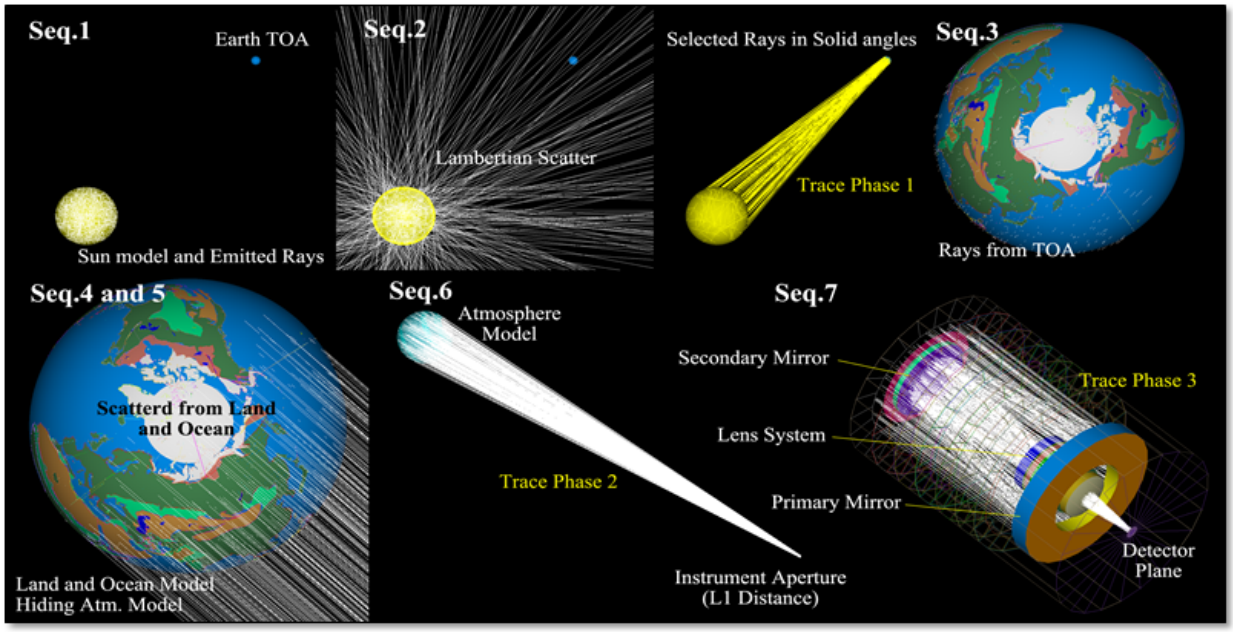

- 슬롯간 복사휘도 편차량의 원인 기작 분석의 일환으로 GOCI 광학계의 잡광 분석 수행(Oh et al. 2013)

  • 한반도 주변 설정 후 육지, 해양 반사율 및 산란 모델 적용 (Ryu et al. 2011)

  a. 지구모델(Earth Model) 구성 시, 해안선을 따라 ASAP 프로그램 상에서 'edge' 명령어 형태도 관측 지역 설정

  b. 위경도 좌표에 대한 GOCI 실제 관측 영역과의 동기화 수행

  c. 육지, 해양 반사율에 대해서는 각 band 별 표준 반사도 값을 사용

  d. 산란모델은, 지표 반사 시 자광선(Child ray)는 3으로 설정, 흩어짐광선(Split ray)는 5로 설정하여, 최대한 지구모델에서 산란되는 경우의 수를 고려함

  • GOCI 광학 시스템 내부의 산란 모델 적용 및 검출기 특성 부여

  a. 산란모델은 Harvey 모델을 사용하였으며, GOCI 개발 당시 적용되었던 흑색 페인트 모델을 적용함

b. 광학계의 특성은 ZEMAX로 설계된 GOCI 광학계를 ASAP으로 도입하였으며, 실제 광학 성능을 기준으로 비교하여 적용

c. 검출기의 수치모사상 위치와 기울기 등은 GOCI 설계 문서를 따라 모델링을 수행함

• 실제와 동일한 스케일을 통한 검출기에서의 영상과 복사량 측정

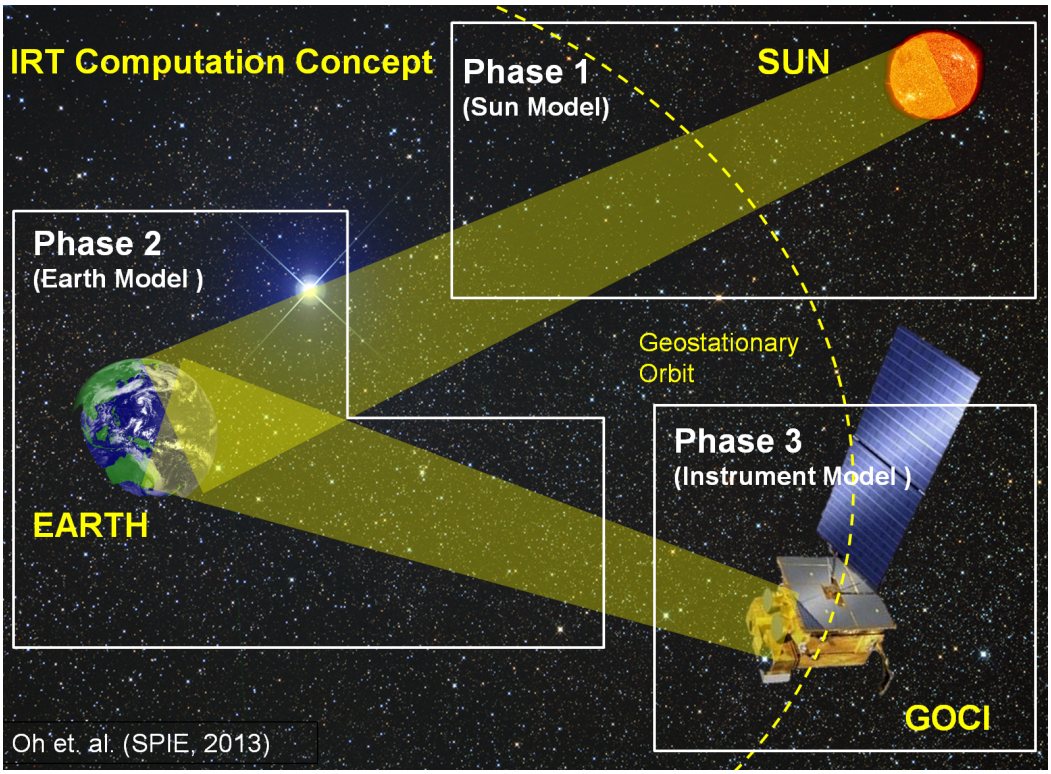

- GOCI 광학계 내 산란값과 잡광 분석(Oh et al. 2013)

• 임계물체(Critical object)와 조명물체(Illuminated object)를 확인하고, 경로별 잡광 가능성 파악

a. 임계물체(빨간색 점)은 3반사경과 열 히터 부근에 유력한 잡광의 원인을 제공하고 있으며, Path 1이 최대 광량(약 93%)을 차지하고 있음

b. 조명물체(파란색 점)은 입사동의 베플 부근의 넓은 면에서 다수 산란되며, 임계물체와 마찬가지로 열 히터 부근이 원인으로 파악됨

c. 경로별로 광량 분포를 파악하였을 때, 필터의 뒷면을 맞고 산란된 광선이 열 히터의 넓은 부분을 맞고 반사되어 검출기로 되돌아 오는 양이 잡광의 다수를 차지함

d. 통합적 광선추적을 위한 기초작업으로 광학계 내 산란 모델 적용을 수행함

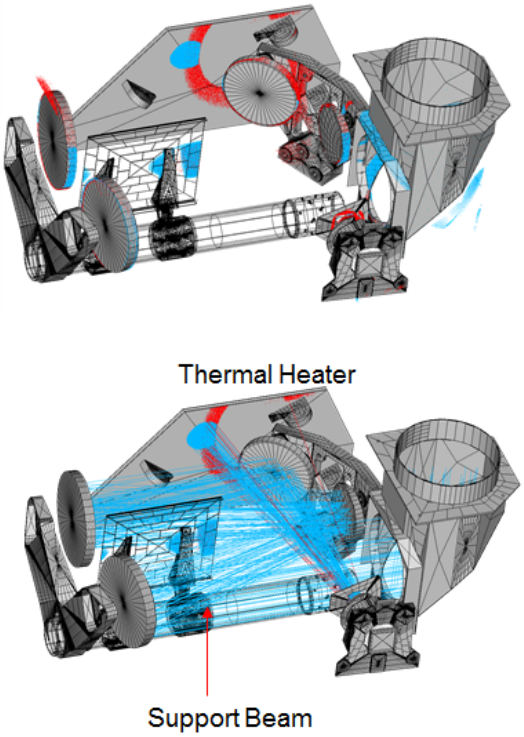

Illuminated Objects				Critical Objects			
Path #	Ray Path[a]	Flux Ratio[b] [%]	Path Description[c]	Path #	Ray Path	Flux Ratio [%]	Path Description
1,2	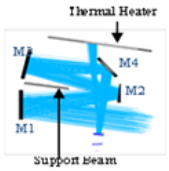	94.3037	Reflected from the Filters (front and back) and sit on the Thermal Heater	1	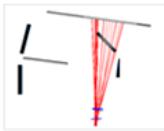	93.3152	Direct transmission through the Window and Filters to reach the Thermal Heater
				4		0.2130	Direct transmission through the Window and Filters, reflected from M2 to reach the Thermal Heater
3,4	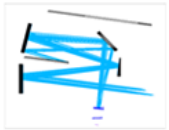	5.3431	Reflected from the Filters (Front and Back), M4 and M3 in order, and sit on the Support Beam	2		4.1177	Direct transmission through the Windows and Filters, reflected from the M4 and M3 in order to reach the Support Beam
5,6	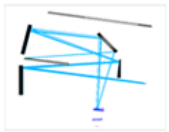	0.2432	Reflected from the Filters (Front and Back) and M4 in order, and sit on the Support Beam	3		2.3542	Direct transmission through the Windows and Filters, reflected from the M4 , M3 and M2 in order to reach the Support Beam

a : the ray history belong to the path number.
b : the relative contribution of each path's flux to the all returned rays
c : rear surface is facing detector along LOS(Line of Sight), while front surface is on the other way.

- IRT를 이용한 궤도상 잡광 분석 및 구름에 의한 잡광 영향 분석(Oh et al. 2013)
  - 궤도상 잡광 분석 수행
    a. 슬롯 별 잡광의 유무 파악
    b. 수치모사상 촬영 각도 정확도 확인
  - 모사된 구름 위치에 따른 잡광의 분포와 정량 분석

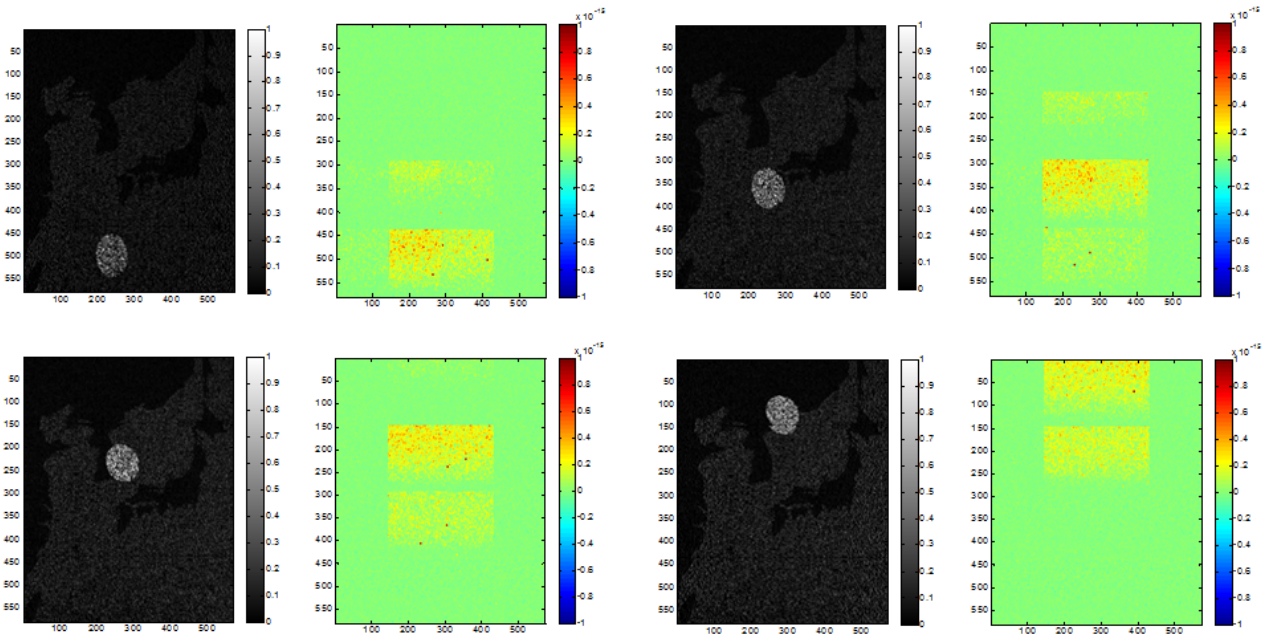

• 구름의 이동에 따른 잡광의 변화 확인 (남-북 방향 변화)

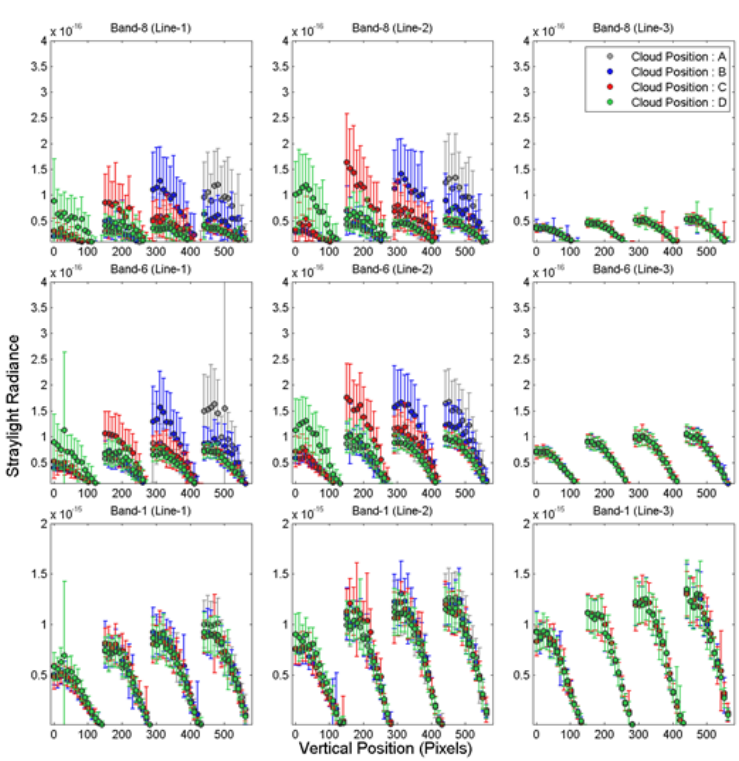

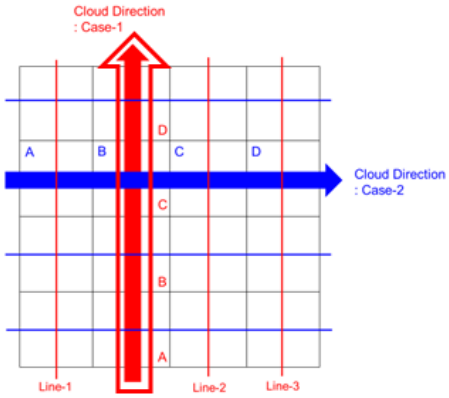

• 구름의 이동에 따른 잡광의 변화 확인 (동-서 방향 변화)

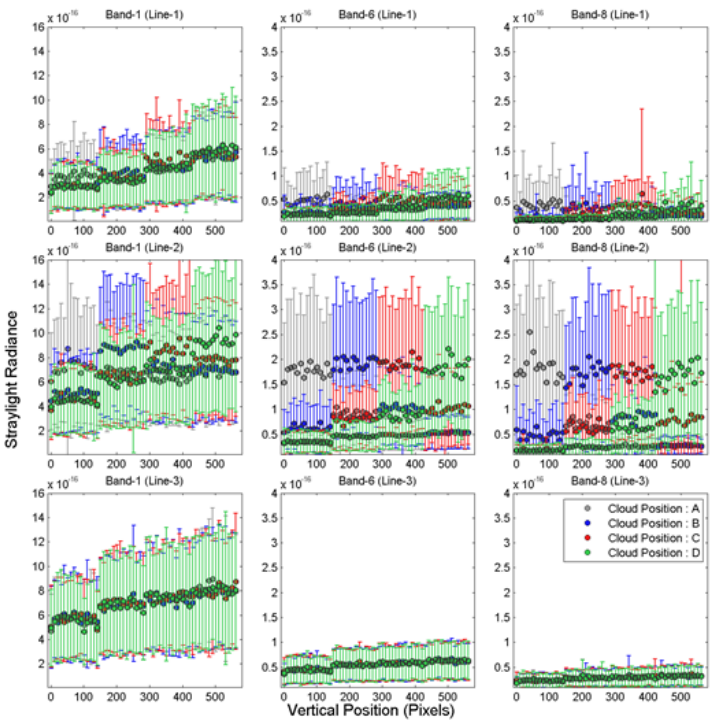

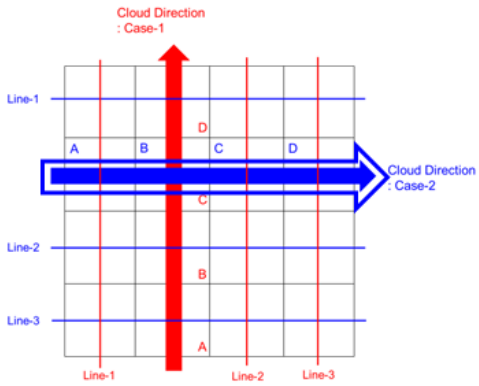

2. 광학 성능 분석 및 보정 기술 개발

- 궤도상 MTF 측정 방법 개선

• 기존의 GOCI 궤도상 MTF 측정 방법 (Oh et al. 2012)

a. 동해안의 해안선을 기준으로 육지와 바다의 경계 MTF 측정 방법 활용

b. 남해안의 500m 이하의 섬을 기준으로 한 점분포함수 적용 방법 활용

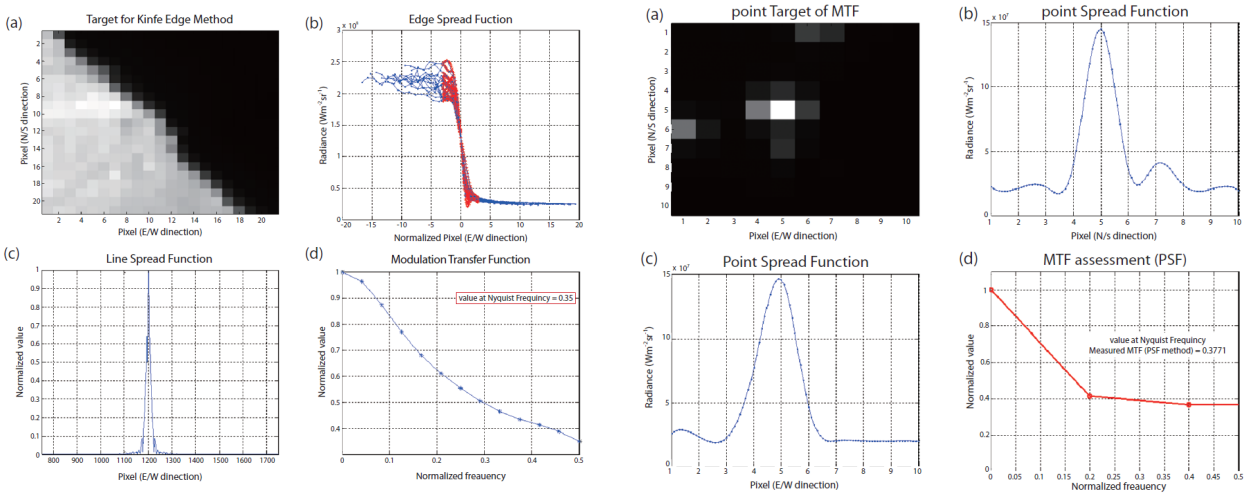

c. 위의 두 방법 모두 자연특성(복사 특성, 환경 요소에 의한 영향)에 따른 큰 오차량을 보이는 단점을 지님

d. 이에 신규 궤도상 측정 방법 고안

• 새만금 방조제를 이용한 MTF 측정 방법 (Oh et al. 2013)

a. 새만금 방조제의 폭을 이용하여 "Pulsed source"로 가정하고, 이를 PSF로 변환하여 MTF 값을 산출함

b. 해외 유수의 기관의 연구 사례에서도 대교를 이용한 방법 등 고해상도 위성 영상에 대한 적용은 많이 이뤄졌으나, 500m급 해상도 영상에 적용은 드물었음

• 새만금 방조제를 이용한 PSF 곡선 산출 후, wiener filter 적용

a. "Pulsed source"로 가정한 방조제의 영상을 PSF로 변환하고, 이 곡선을 Gaussian curve로 피팅하여 MTF 값의 신뢰도를 향상시킴

b. Wiener Filter에 적용하기 위하여, SNR 값은 동해안의 노이즈가 적은 영역을 산정하

여 산출하고, PSF 값과 더불어 필터를 완성시킴

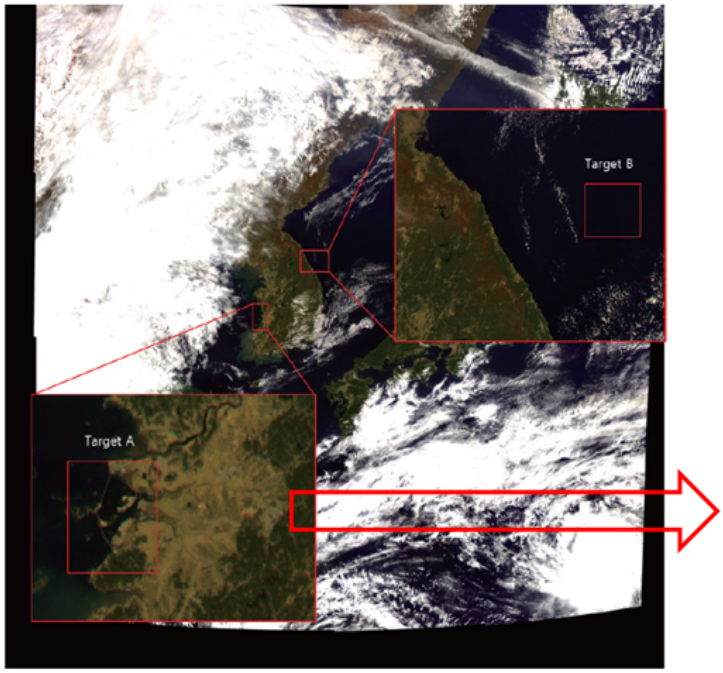

Fig. 2. Target areas. Target A and B are for calculating PSF value and SNR respectively.

Oh et. al. (JASS, 2013)

$$g(x) = \frac{1}{\sigma\sqrt{2\pi}} e^{\frac{1}{2}(\frac{x-\mu}{\sigma})^2}$$

$$W(u,v) = \frac{S^*(u,v)}{|S(u,v)|^2 + \frac{c\Phi_N(u,v)}{\Phi_O(u,v)}} = \frac{S^*(u,v)}{|S(u,v)|^2 + \frac{1}{SNR}}, (c=1)$$

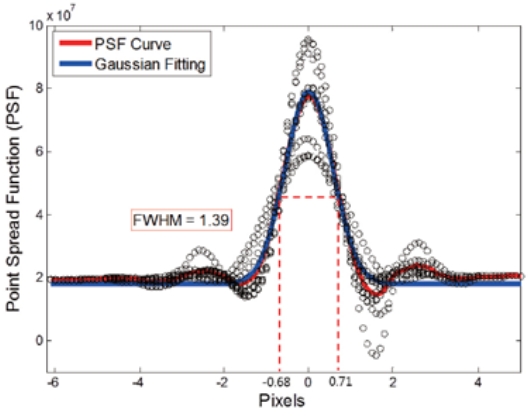

- Wiener 필터를 이용한 결과 영상 품질이 향상됨
  a. 방조제 영상은 물론 GOCI 전체의 Sharpness가 향상되었음
  b. 정량적으로도 원래 영상에 비하여 MTF 성능이 35.06% 향상됨

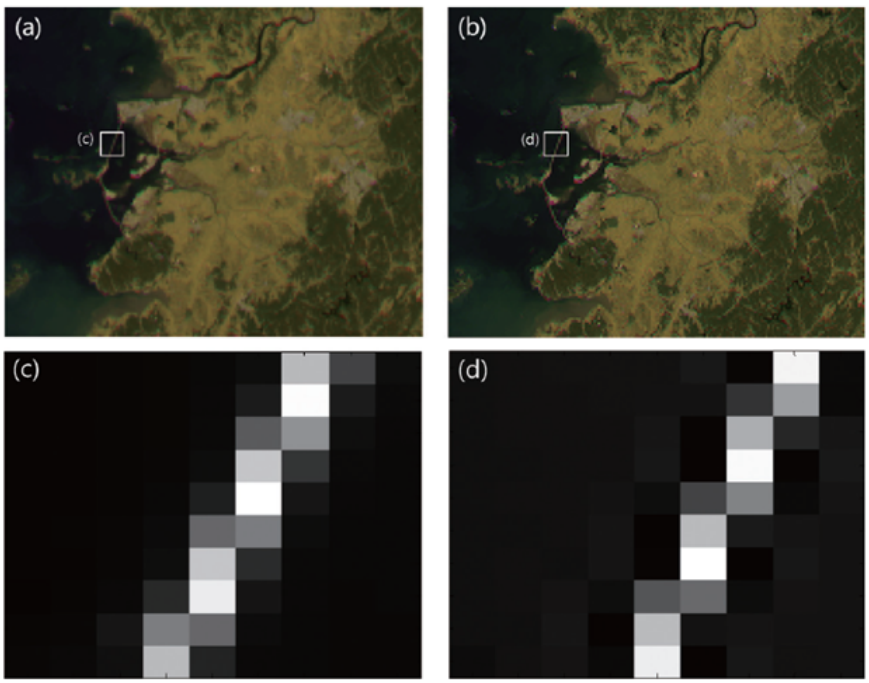

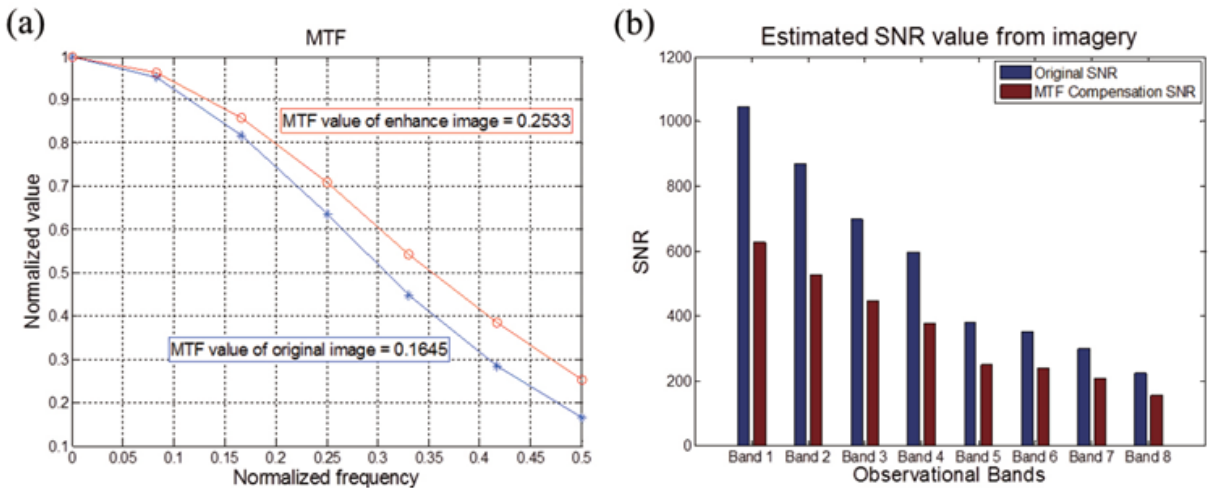
(a)
MTF
MTF value of enhance image = 0.2533
MTF value of original image = 0.1645
Normalized value
Normalized frequency
(b)
Estimated SNR value from imagery
Original SNR
MTF Compensation SNR
SNR
Band 1
Band 2
Band 3
Band 4
Band 5
Band 6
Band 7
Band 8
Observational Bands

제 2 절 2차년도 연구개발 수행 내용

1. GOCI 영상 성능(MTF)의 궤도상 측정 및 보정 기법 개발

- GOCI 센서의 열화(Degradation)에 의하여 영상의 선명도(Sharpness)가 저하되는 영향을 보정하는 기법
  - Wiener 필터의 설계 시 Gaussian factor의 상관관계 분석
    a. 최적의 Gaussian factor(0.4) 값을 도출하고, 영상 보정에 적용
    b. MTF 영상의 향상과 더불어 해색 산출물의 정확도가 저하되지 않는 범위를 도출
    c. 서해 연안의 영상(경기만 지역)을 토대로 검증함
- 영상의 에지 영역(해안선, 연안 등)에서 보다 효율적으로 활용이 가능함
  - Wiener 필터의 적용을 통해 기타 해색 산출물에 적용 수행 (Ocean Front 등)
    a. 원 영상에서의 노이즈 제거는 물론, 경계 부근의 Sharpness가 향상됨
    b. 동해 지역에 대하여 적용한 결과, 에디 등의 해양 현상이 명확하게 확인됨

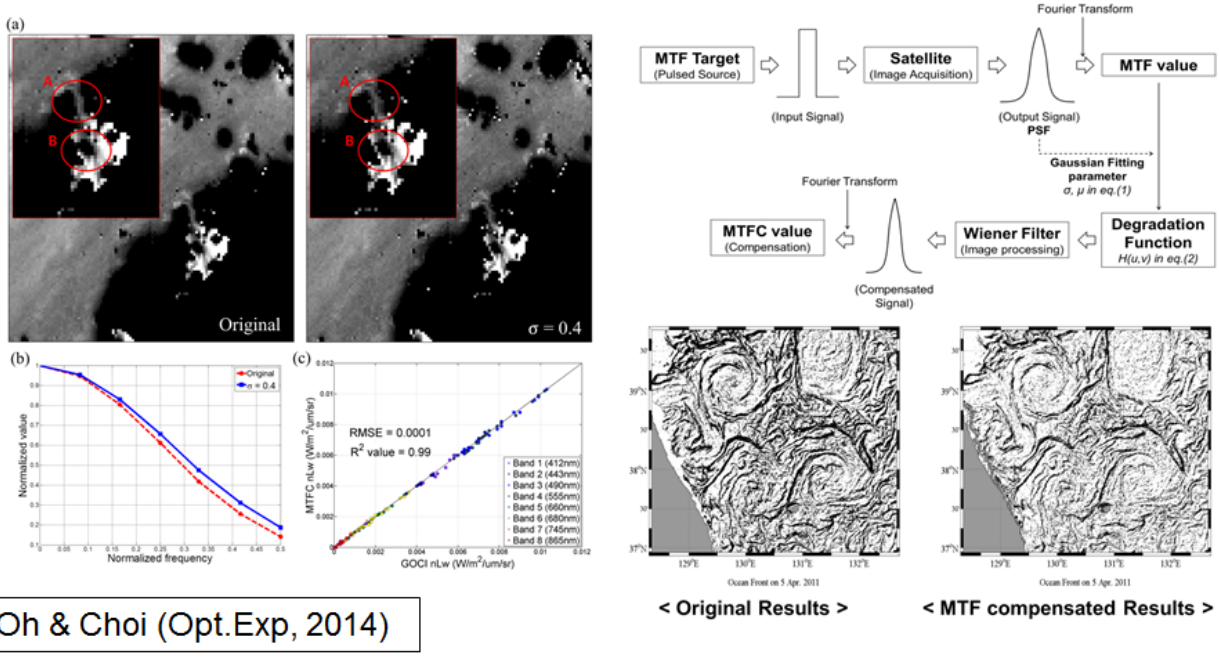

Oh & Choi (Opt.Exp, 2014)

2. 통합적 광선추적기법을 이용한 광학복사 능력 검증

- 1차년도에 수행하였던 기초적인 광선추적 기반 잡광해석 기술의 고도화
  - GOCI의 기기적 잡광 요인을 분석하고, 해상도가 증가된 지구모델을 도입
    a. 기기적인 잡광 영향을 별도로 분석
    b. 육지 및 해양의 반사도 차이에 따른 잡광 영향 고려
    c. 수치모사된 구름(반사도가 높은 타겟)을 설정하여, 주변 슬롯에 미치는 영향 확인

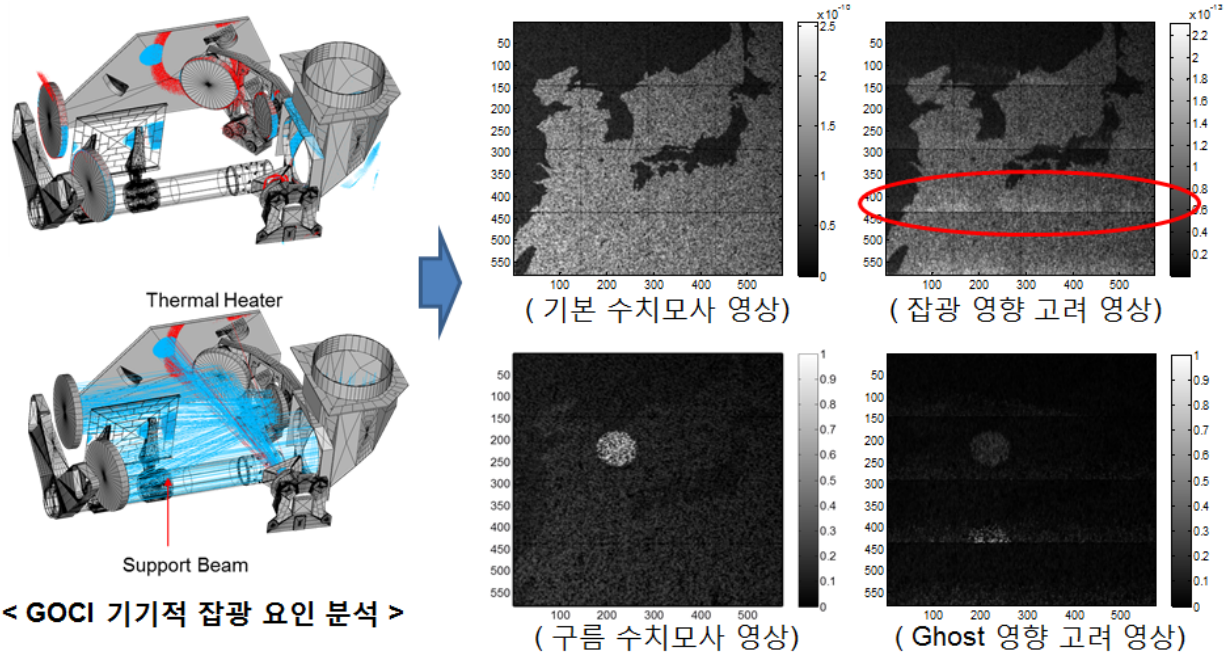

< GOCI 기기적 잡광 요인 분석 >

- 슬롯 별, 잡광 비율 매트릭스(matrics) 구성

  • GOCI 영상과 동일한 화소수로 잡광 비율을 모사

  a. 구름 환경 및 변화량에 따른 밴드별 특성 고려

  b. 밴드 특성(필터의 구성 및 각도 변화)에 따른 잡광 비율의 차이를 확인

  c. 주변 슬롯에 미치는 영향(상-하, 좌-우)의 원인 분석 수행

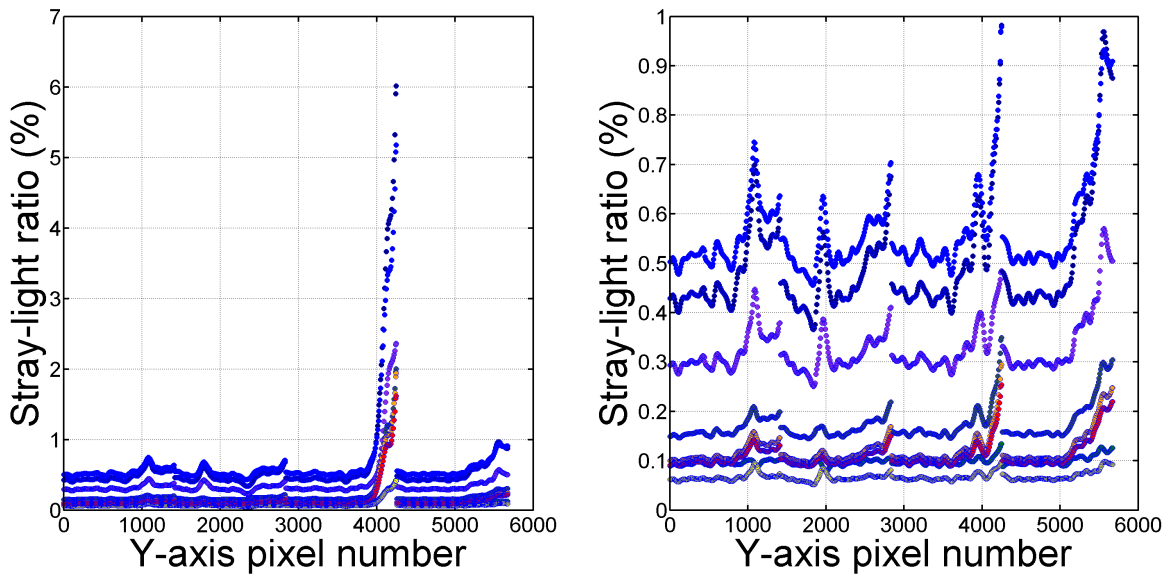

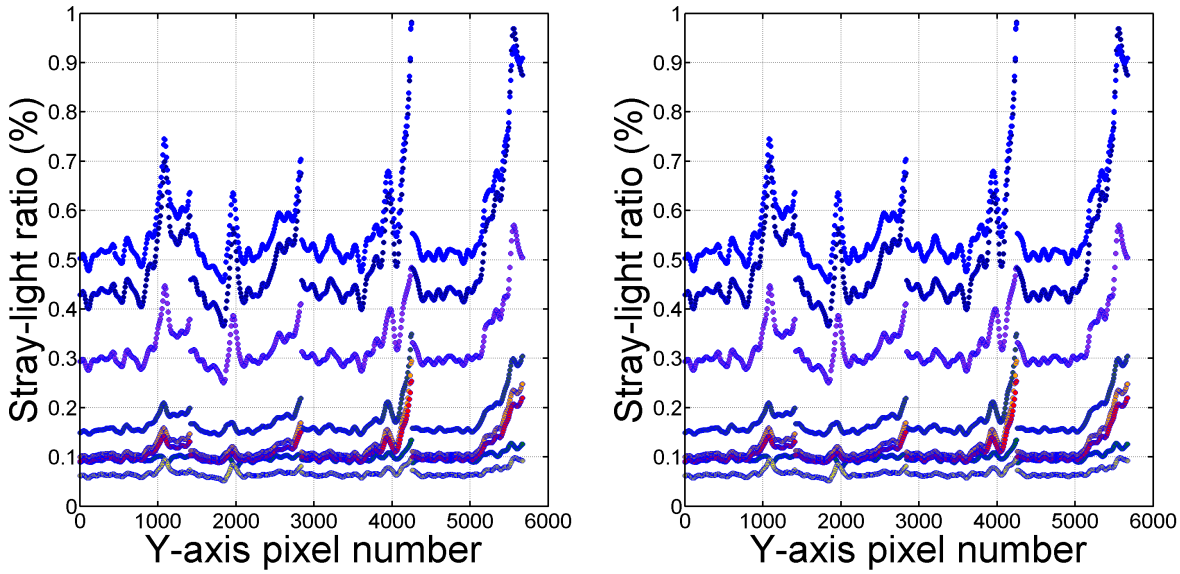

3. 잡광 요인을 최소화하는 광학 설계를 위한 정렬 기법 구현

- 민감도법을 이용한 정밀 정렬 기술 개발, S/W 구현 및 실험적 검증 수행
  - Zernike 계수의 민감도를 이용한 광학기기의 정렬 기법 구현
  - GOCI와 유사한 반사 광학계에 대하여 실험적 적용
- Merit Function을 이용한 정밀 정렬 기술와의 비교 연구 수행
  - GOCI와 유사한 3반사 광학계에 대하여 실험적 적용

▶ 정렬 대상 광학계

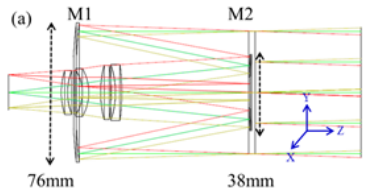

▼ 정렬 실험 결과

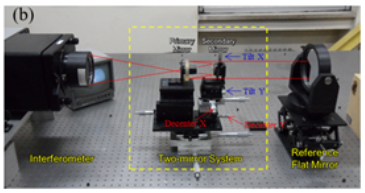

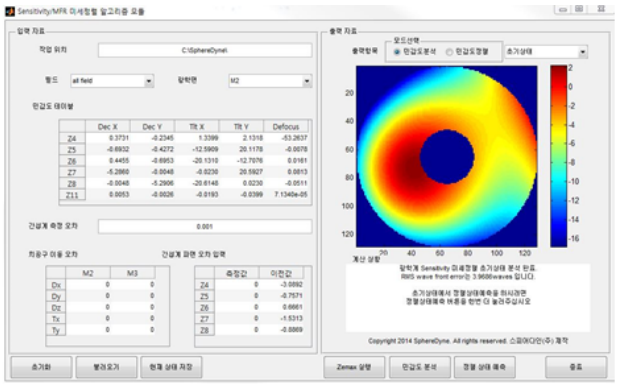

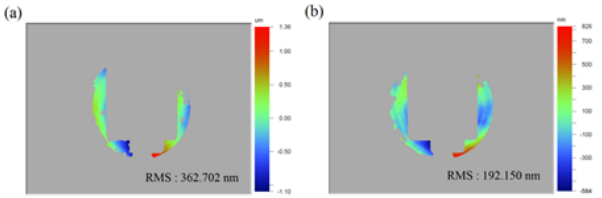

▲정렬 알고리즘 구현 S/W

Oh et. al. (JASS, 2014)

4. GOCI 영상의 복사검증을 위한 해수용 BRDF 측정장비 개발 및 초기 결과 도출

- BRDF 측정 장비 개발

  • 기존의 고체 시료에 대한 BRDF 측정 장비 변형

  • GOCI와 유사한 반사 광학계에 대하여 실험적 적용

❖ **Experimental Set-Up**

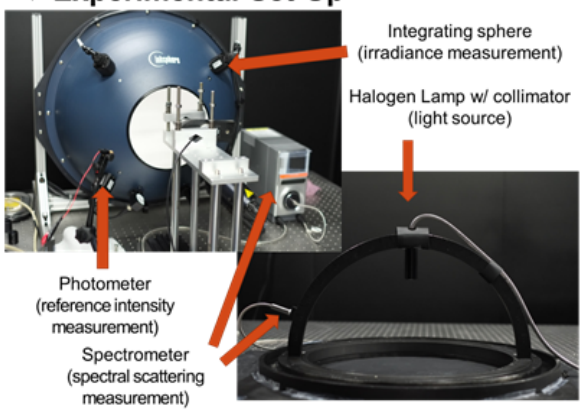

$$BRDF = \frac{\Phi_s / \Omega}{\Phi_i \cos\theta_s}$$

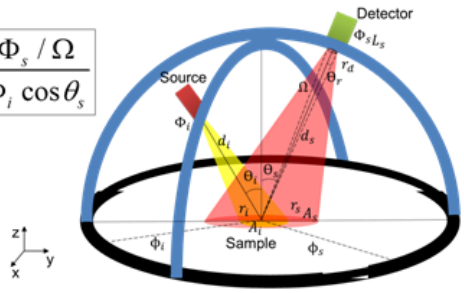

Oh et. al. (SPIE, 2014)

	Case 1 : Spectralon	Case 2 : Clear Water	Case 3 : Turbid Water
0°	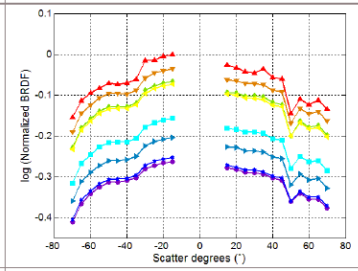	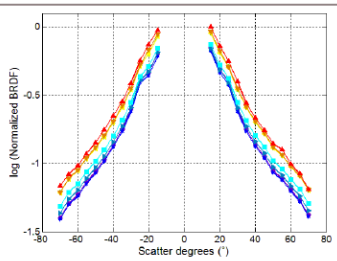	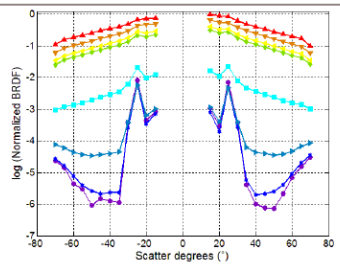
30°	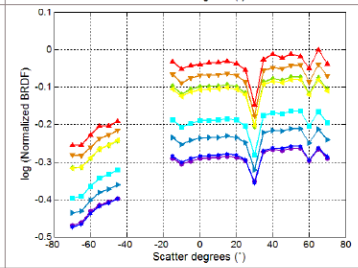	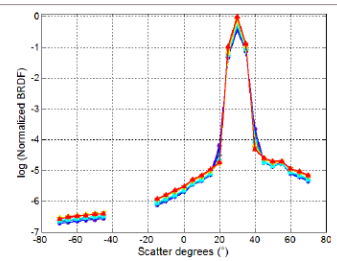	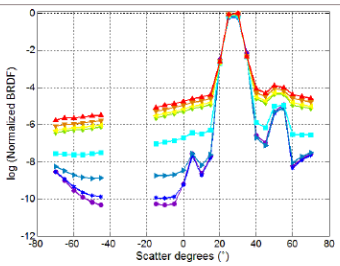
60°	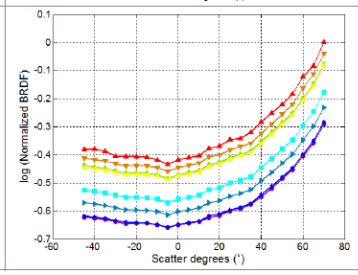	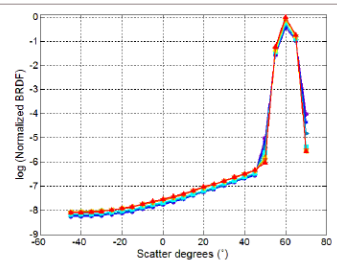	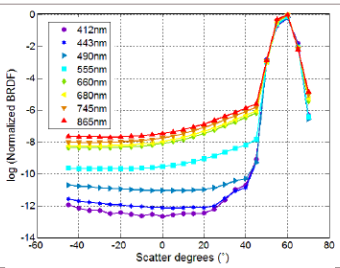

제 4장 연구개발목표 달성도 및 대외기여도

제 1 절 연구목표 달성도

성과목표(가중치)		평가의 착안점 및 척도	최종목표 달성도
1차년도 (2013)	○ GOCI에 대한 광선 추적 기반의 광학 성능 평가 시스템 구축의 선행연구 (30%)	○ 태양 모델을 통한 광원 설정 하였는가? ○ 한반도 주변 설정 후 육지, 해양 반사율 및 산란 모델 적용 하였는가? ○ GOCI 광학 시스템 내부의 산란 모델 적용 및 검출기 특성 부여 하였는가? ○ 실제와 동일한 스케일을 통한 검출기에서의 영상과 복사량 측정 하였는가?	100%
	○ 이미지 기반 성능평가 (25%)	○ 광선 추적 기법과 지향 반사경의 운용 시스템을 적용 하였는가? ○ 슬롯 별 광선 추적 후 영상 처리 적용하였는가? ○ 슬롯 별 광원 모델과 특정한 주변 영향에 대한 영상 수치모사 하였는가?	100%
	○ GOCI를 통한 원격탐사 용 수치모사 시스템 선행연구 (25%)	○ 한반도 해역에 대한 지구모델과 GOCI의 실 운용 시스템을 접목 시킨 원격탐사 형태의 수치모사 수행 하였는가? ○ Monte-Carlo 방식을 이용한 통계적 수치모사 수행 하였는가?	100%
	○ 궤도상 GOCI 광학 시스템 내 잡광 분석 (20%)	○ GOCI 시스템 내부 산란 특성 분석 하였는가? ○ 잡광 요인 분석 및 정량적인 잡광과 Ghost 량 추이 분석 하였는가? ○ Step & Stare 방식에서의 주변 슬롯에 의한 잡광 분석 하였는가? ○ 잡광 분석을 통한 영상에서의 잡광 분포를 통한 영상 재조합 수행 하였는가?	100%
2차년도 (2014)	○ 통합적 광선추적 기법을 이용한 광학 복사 능력 검증 (30%)	○ GOCI의 궤도상 잡광 분석이 이루어졌는가? ○ 광학 시스템 틀어짐에 따른 잡광 형태 변형 및 정량적 분석되었는가? ○ 통합적 광선추적 기법의 성능 검증을 수행하였는가?	100%
	○ 광학계 정렬 기법 수치모사를 통한 시스템 성능 검증 (25%)	○ 다중 설계 최적화 방법을 이용한 GOCI의 광학계 정렬해 분석을 수행하였는가? ○ GOCI-II 광학계의 최적 정렬 방법을 구성하였는가? ○ 정렬 기법 구현 프로그램 구축하였는가?	100%
	○ 영상처리 수치모사를 이용한 영상 품질 향상 (25%)	○ Wiener 필터를 이용한 MTF 보상 기법을 구성하였는가? ○ MTF 보상 결과와 해양 산출물의 정확도 상관관계 분석 하였는가?	100%
	○ BRDF 측정 시스템 개발을 통한 수치모사 정확도 향상 (20%)	○ 해수 BRDF 측정 시스템 설계 및 구축 하였는가? ○ 적분구의 불확도 측정 시험 하였는가? ○ 해양 관측 장비의 수중 스펙트럼 수치모사를 적용하였는가?	100%
합계(100%)			100%

제 2 절 연구개발 과제의 학술적 성과

1) 논문게재 성과

게재일	논문명	저 자			학술지명	Vol. (No.)	국가명	SCI 구분
		주저자	교신저자	공동저자				
13.12.10	A Modulation Transfer Function Compensation for the Geostationary Ocean Color Imager (GOCI) based on the Wiener Filter	오은송	조성익	안기범, 유주형	Journal of Astronomy and Space Sciences	30(4)	한국	학진
14.7.14	현장관측용 분광광도계의 상대검교정 시스템 개발	오은송	박영제	안기범, 강혁모, 조성익	대한원격탐사학회지	30(4)	한국	학진
14.9.4	Experimental Sensitivity Table Method for Precision Alignment of Amon-Ra Instrument	오은송	김석환	안기범	Journal of Astronomy and Space Sciences	31(3)	한국	학진
14.10.22	GOCI image enhancement using an MTF compensation technique for coastal water applications	오은송	최종국		Optics Express	22(22)	미국	SCI

2) 논문발표 성과

발표일	논문명	저 자		학술회의명	국내외 구분
		주발표자	공동발표자		
13.5.27	Construction of digital elevation map(DEM) integrated earth system optical model	류동옥	성세현, 오은송, 김석환	2013 춘계 한국우주과학회 학술대회	국내
13.5.27	Ray Tracing Based Simulation of Stray Light Correction for Geostationary Ocean Color Imager	오은송	홍진석, 안기범, 조성익, 유주형, 김석환	2013 춘계 한국우주과학회 학술대회	국내
13.8.29	Ray Tracing based simulation of stray light effect for Geostationary Ocean Color Imager	오은송	홍진석, 안기범, 조성익, 유주형, 김석환	2013 SPIE (Optics+Photonics)	국외
13.8.29	Backward Reflection Analysis of Transmitting Channel of Active Laser Ranging optics	홍진석	오은송	2013 SPIE (Optics+Photonics)	국외

13.10.23	A Modulation Transfer Function Compensation for the Geostationary Ocean Color Imager(GOCI) based on the Wiener Filter	오은송	안기범, 조성익, 유주형	2013 추계 한국우주과학회 학술대회	국내
14.04.17	Radiometric calibration experiment of the field campaign equipment for GOCI data validation	오은송	강혁모, 안기범, 조성익, 박영제	International Symposium on Remote Sensing 2014	국내
14.4.21	An optimal sharped GOCI Imager for coastal water with MTF compensation	오은송	최종국	2014 춘계 한국우주과학회 학술대회	국내
14.4.21	Development Progress of Ocean Color Sensor Based on UAV : Design and Performance of TMA Optical System	오은송	강혁모, 현상원, 김건희, 박영제, 김석환	2014 춘계 한국우주과학회 학술대회	국내
14.4.21	Alignment state estimation simulation of Korsch type telesope based on DDE programming	강혁모	오은송, 류동옥, 한정열, 김석환	2014 춘계 한국우주과학회 학술대회	국내
14.8.19	Preliminary design of multi-spectral BRDF measurement system for water surface	오은송	강혁모, 양슬기, 김석환, 박영제,	2014 SPIE (Optics+Photonics)	국외
14.10.29	Performances of CAA Algorithms for Alignment State Estimation Simulations for Three-mirror Anastigmat Earth Observation Optical System	강혁모	오은송, 현상원, 김건희, 박영제, 김석환	2014 추계 한국우주과학회 학술대회	국내
14.10.16	해수 현장 관측용 분광 광도계간 상대 교정 연구	강혁모	오은송, 문정언, 박영제	2014 추계 대한원격탐사학회	국내

3) 특허성과

출원된 특허의 경우				
특허명	**발명자**	**출원일**	**출원번호**	**출원국가**
정지궤도 해양관측센서의 궤도상 잡광 해석을 위한 모델의 구성방법	오은송, 홍진석	2013-10-17	10-2013-0123809	대한민국
웨이퍼 에지 노광용 시준기 설계	오은송	2014-10-31	10-2014-0150459	대한민국

제 5 장 연구개발결과의 활용계획

제 1 절 기대효과

가. 기술적 측면

○ 현재 운용 중인 GOCI의 궤도상 성능 검증을 함으로써 해양 관측 임무 수행에 안정적인 자료 제공

○ 궤도상 잡광 분석을 전우주적 관점에서 수행하는 세계 최초의 연구를 수행하므로 써 정지궤도뿐만 아니라 저궤도, 항공용 탑재체의 운용 중 궤도상 잡광의 영향을 파악할 수 있는 기술을 개발

○ 차세대 해양관측 위성의 초기 개념 설계부터 광기계부 설계에 이르기 까지 End-to-end 수치모사 시스템을 구축하므로 써 시간과 개발 비용을 절약할 수 있으며, 월등한 요구사항을 지니는 차세대 해양관측 위성의 안정적인 개발을 가능하게 함

나. 경제 산업적 측면

○ 본 연구 결과로 얻게 될 광선 추적 기반 정지궤도 해양탑재체 수치모사 시스템은 곧바로 현재 GOCI 활용 연구에 직접적으로 사용될 수 있으며, 추후 GOCI-II 개발에 있어서 성능 평가 및 향상에 기여하므로 써, 국내 우주개발 산업의 기술력을 배가시킬 것으로 예상됨

제 2 절 타 활용방안

○ 현재 운용 중인 GOCI 영상의 활용성을 향상

- 잡광 분석 기법을 통한 영상 처리를 수행하여 해양 산출물의 정확도를 향상
- MTF 보상 기법을 이용한 영상 처리 원천 기술 확보
- 광학 탑재체와 위성 영상간의 상관성 연구를 통한 실질적인 활용 방안 모색

○ 차세대 해양관측위성의 궤도상 성능 예측 시스템 도입을 통한 사용자 요구사항의 타당성 검토

- 본 사업의 결과물을 토대로 추후 발전적인 연구 방향으로 지속 연구할 계획

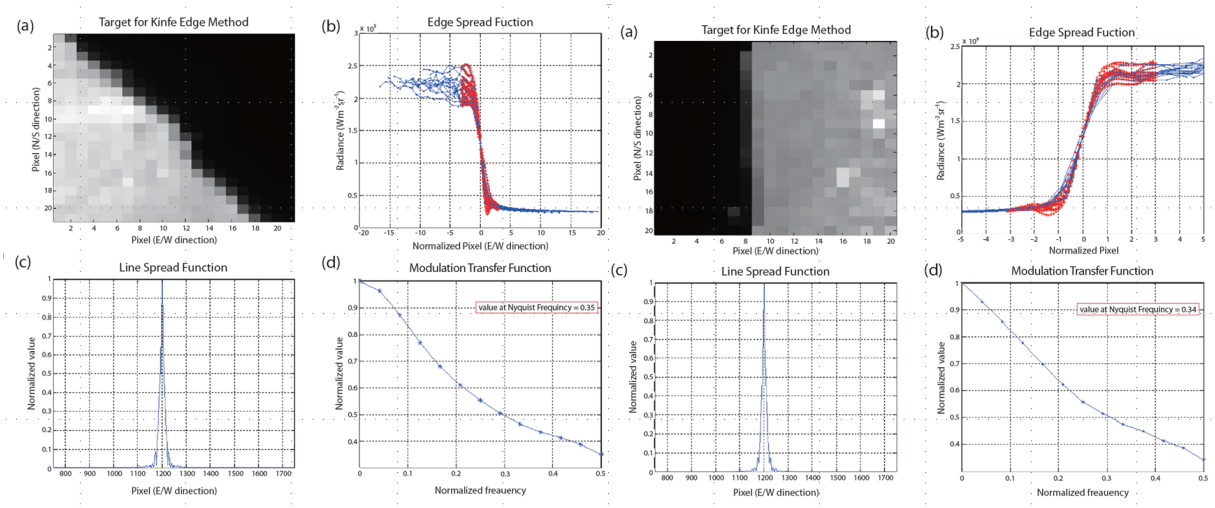

그림 6. GOCI 궤도상 MTF 성능 검증 예시

○ 원격탐사 연구 중 육지 및 해양의 분광 수치모사 연구 수행

- 중장기적 연구 목표로써, Hyperspectral 센서의 활용 등 각종 수치모사에 있어 지속적인 연구를 수행할 계획

- 신진 연구자 사업에서의 결과물은 추후 분광 수치모사 연구의 선행연구로써 가치가 있을 것으로 예상됨

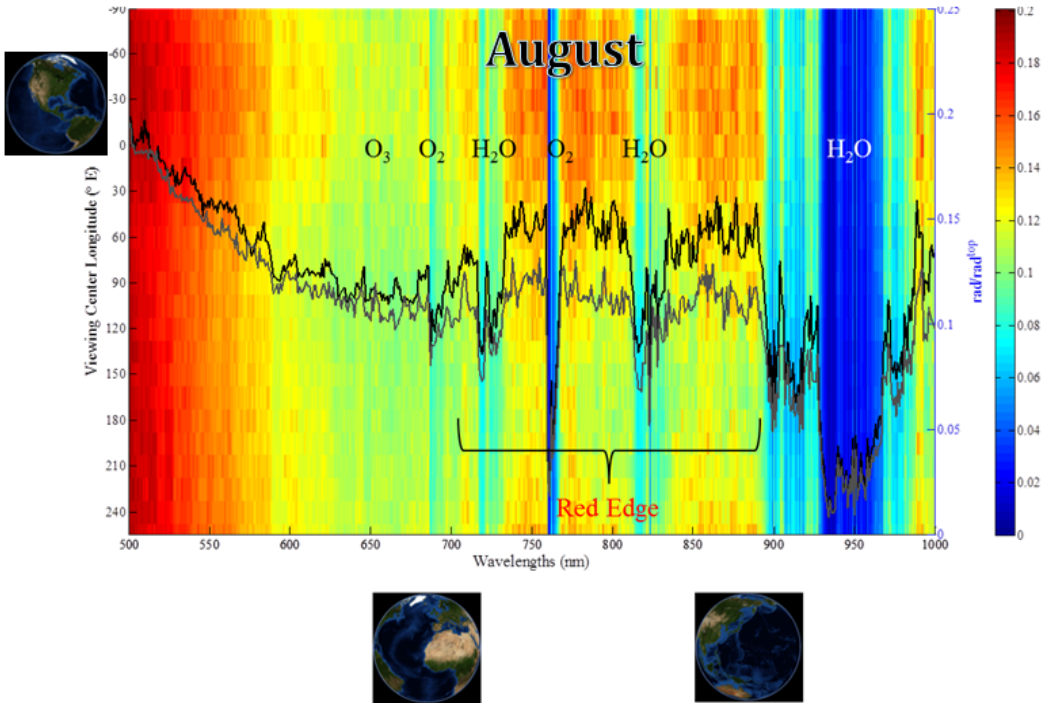

그림 7. 육지의 BSDF 특성을 고려한 산란 모델 적용 후 광선 추적 기반 End-to-End 수치모사 연구

○ 수치모사 시스템 구축 및 정확도 향상을 위한 실험 기반 구축

- 현장관측 장비 검교정 및 장비의 광특성 수치모사를 수행하므로써, 현장 관측 시 발생할 수 있는 오차 점검

- BRDF 측정 장비 구축으로 해수 및 각종 시료의 광특성 분석을 통해 수치모사 라이브러리 구축 가능

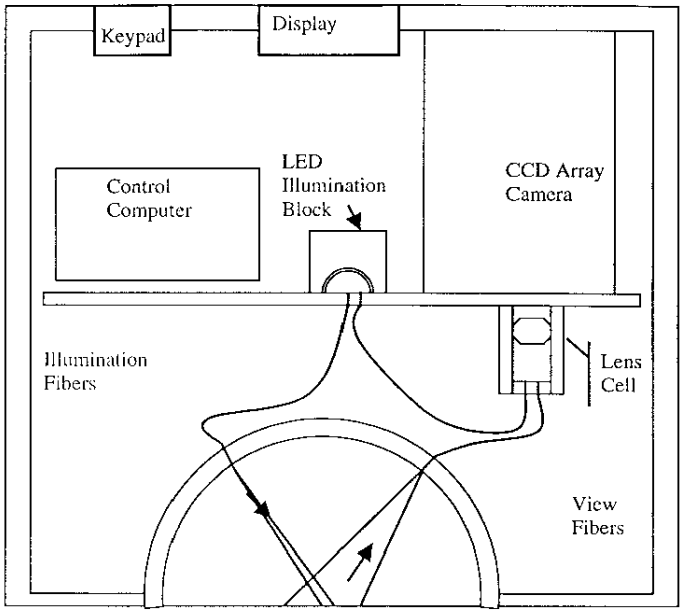

Fig. 2. Diagram of instrument design with major components listed.

그림 8. 선진연구기관의 BRDF 측정 장비 개략도 (Kenneth, J.V. et al., 2000)

제 6 장 참고문헌

1. K. Segl, L. Guanter and H. Kaufmann "Simulation of spatial sensor characteristics in the context of the EnMAP hyperspectral mission", IEEE Trans. Geosci. Remote Sens., vol. 48, pp.3046 -3054 (2010).

2. Nikita S. Pougatchev, "Validation of atmospheric sounders by correlative measurements," Appl. Opt. 47(26), pp. 4739-4748 (2008).

3. D. Ryu, S.-W. Kim, and S. Seong, "Improved Atmospheric 3D BSDF Model in Earthlike Exoplanet using Ray-tracing Based Method," Proc. of SPIE 8521, 8521F-1-9 (2012).

4. S. Seong, J. Yu, D. Ryu, J. Hong, J.-Y. Yoon, S.-W. Kim, J.-H. Lee, and M.-J. Shin, "Imaging and radiometric performance simulation for a new high performance dual band airborne reconnaissance camera," Proc. of SPIE 7307, 730705-1-13 (2009).

5. E. Oh, J. Hong, S.-W. Kim, S. Cho, J.-H. Ryu, "Ray Tracing based simulation of Stray light effec for Geostationary Ocean Color Imager," Proc. of SPIE 8840, 884006-1-8 (2013).

6. E. Oh, K.-B. Ahn, S. Cho, and J.-H. Ryu, "A Modulation Transfer Function Compensation for the Geostationary Ocean Color Imager (GOCI) Based on the Wiener Filter," JASS 30(4), 321-326(2013)

7. E. Oh, K.-B. Ahn, H. Kang, S. Cho, and Y.-J. Park, "Development of relative radiometric calibration system for in-situ measurement spectroradiometers," KJRS 30(4), 455-464(2014).

8. E. Oh and J.-K. Choi, "GOCI image enhancement using an MTF compensation technique for coastal water application," Opt. Express 22(22), 26908-26918(2014)

9. E. Oh, K.-B. Ahn, and S.-W. Kim, "Experimental Sensitivity Table Method for Precision Alignment of Amon-Ra Instrument," JASS 31(3), 241-246(2014)

별첨 1. 주요 성과 : 논문

Technical Paper
J. Astron. Space Sci. 30(4), 321-326 (2013)
http://dx.doi.org/10.5140/JASS.2013.30.4.321

JASS Journal of Astronomy and Space Sciences

A Modulation Transfer Function Compensation for the Geostationary Ocean Color Imager (GOCI) Based on the Wiener Filter

Eunsong Oh[1,2], Ki-Beom Ahn[1,2], Seongick Cho[1,2†], Joo-Hyung Ryu[1]
[1]Korea Ocean Satellite Center, Korea Institute of Ocean Science and Technology, Ansan 426-744, Korea
[2]Space Optics Laboratory, Dept. of Astronomy, Yonsei University, Seoul 120-749, Korea

The modulation transfer function (MTF) is a widely used indicator in assessments of remote-sensing image quality. This MTF method is also used to restore information to a standard value to compensate for image degradation caused by atmospheric or satellite jitter effects. In this study, we evaluated MTF values as an image quality indicator for the Geostationary Ocean Color Imager (GOCI). GOCI was launched in 2010 to monitor the ocean and coastal areas of the Korean peninsula. We evaluated in-orbit MTF value based on the GOCI image having a 500-m spatial resolution in the first time. The pulse method was selected to estimate a point spread function (PSF) with an optimal natural target such as a Seamangeum Seawall. Finally, image restoration was performed with a Wiener filter (WF) to calculate the PSF value required for the optimal regularization parameter. After application of the WF to the target image, MTF value is improved 35.06%, and the compensated image shows more sharpness comparing with the original image.

Keywords: modulation transfer function, MTF compensation, Wiener filter, geostationary ocean color imager (GOCI)

1. INTRODUCTION

The world's first geostationary ocean remote-sensing instrument, the Geostationary Ocean Color Imager (GOCI), was launched on 27 June 2010 to monitor the marine environment of the Korean peninsula. GOCI provides eight image acquisitions a day for the Northeast Asian region and can be applied to various research areas, such as suspended sediment and chlorophyll concentration monitoring, in addition to providing timely warning of marine dangers. GOCI images have a 500-m spatial resolution, consisting of 16 slot images for a 2500 × 2500 km area, centered at 130°E, 36°N (Table 1) (Ryu et al. 2012). Calibration and image quality control and enhancement are crucial to the successful operation of the GOCI system. The precise image quality assessment for increasing the applicability and scientific data accuracy uses a modulation transfer function (MTF) and signal-to-noise ratio (SNR) comparison.

In image-based MTF measurement methods, the knife-edge method, point source method, and pulse method are widely used to determine whether the targeted optical system performance has been achieved in real instrument operation. These methods also account for factors influencing the space environment which can change the resulting image quality (Helstrom 1967, Holst 2008, Hwang et al. 2008, Viallefont 2010, Yin et al. 1990). A common concept among the three methods is the characterization

Table 1. General specifications of the Geostationary Ocean Color Imager (GOCI).

Items	Specification
Volume (mm^3)	1,000 × 760 × 896
Weight (kg)	< 83.3
Spatial resolution (GSD)	500 m @ point of 130°E, 36°N
Observation period	1 hour (8 times per day)
MTF requirement	> 0.3 @ Nyquist frequency
SNR requirement	> 1,000

Received Sep 7, 2013 **Revised** Nov 13, 2013 **Accepted** Nov 26, 2013
†Corresponding Author
E-mail: sicho@kiost.ac
Tel: +82-31-400-7787, Fax: +82-31-400-7715

http://janss.kr pISSN: 2093-5587 eISSN: 2093-1409

of the spatial quality of the remote-sensing systems with the Fourier transform of the point spread function (PSF) of the target image. First, the knife-edge method uses an edge spread function (ESF) created by a well-contrasted edge area in the target image. The line spread function (LSF) is then computed by a simple discrete differentiation of the ESF; the MTF value is obtained by the Fourier transform of the LSF in the last step (Choi 2002, Viallefont 2010, Viallefont & Leger 2010). The other two methods, the point source and pulse methods, are similar to the knife-edge method, but these methods obtain the PSF values directly from a particular point source and pulse. In this case, the MTF value is computed by Fourier transformation of the PSF (Choi 2002, Leger et al. 1994).

In this study, we focused on the proper MTF estimation method using the natural target and GOCI image enhancement with MTF compensation. If we assume that the remote-sensing PSF blurs the acquired image caused by atmospheric effects, satellite conditions, and other space environment effect, then MTF compensation methods are usually used to correct image degradation with estimating blurred PSF. These MTF compensation methods include the use of an inverse filter (IF), a pseudo-inverse filter (PIF), and a Wiener filter (WF) (Demoment 1989, Jeon et al. 2012). Despite the aforementioned techniques developed and used for various remote-sensing image investigations (Reichenbach et al. 1995, Rojas et al. 2002, Ruiz & Lopez 2002, Wu & Schowengerdt 1993), image enhancement for GOCI has never been studied with MTF compensation using the Wiener Filter.

This paper begins with a description of the GOCI system, MTF estimation, and compensation technique in Section 1. The methodology used to estimate MTF with the pulse method and image enhancement by Wiener filtering as compensation is described in Section 2. Section 3 presents the enhanced image results with MTF compensation for the Saemangeum area. Conclusions are presented in Section 4.

2. METHODS

2.1 Image-based MTF assessment method: pulse method

Fig. 1 shows the general process of MTF assessment, using the pulse method. First, a PSF value is obtained from the pulse target in an acquired image. The image is then Fourier transformed from a PSF to an MTF value (Helstrom 1967). The target area for the pulse input signal should be smaller than the spatial resolution of the remote sensor. The MTF result is more accurate when the Nyquist frequency is less than the first zero-crossing frequency in the Fourier transform step (Tzannes & Mooney 1995). Fig. 1 shows the blurring of an image of a rectangular-shaped input pulse, due to environmental effects, resulting in a PSF value that has a curve-shaped output. The pulse shape is determined by the size of the target pulse width. However, because noise is included in the pulse signal, a PSF curve-fitting model should be applied, such as the Gaussian function, polynomial curve, or Fermi function, which are commonly used for this purpose (Choi 2002, Jo et al. 2008, Smith 2006). For this study, we used a Gaussian function to fit the PSF curve, defined by

$$g(x)=\frac{1}{\sigma\sqrt{2\pi}}e^{-\frac{1}{2}(\frac{x-\mu}{\sigma})^2} \quad (1)$$

where σ and μ are the standard deviation and median value of the Gaussian curve, respectively. These two parameters will be used in the principle values of the WF.

2.2 Remote-sensing image compensation method: Wiener filter (WF) method

The purpose of image restoration is to remove noise from remote-sensing images and to approximate the original image via estimation with an ideal degradation model.

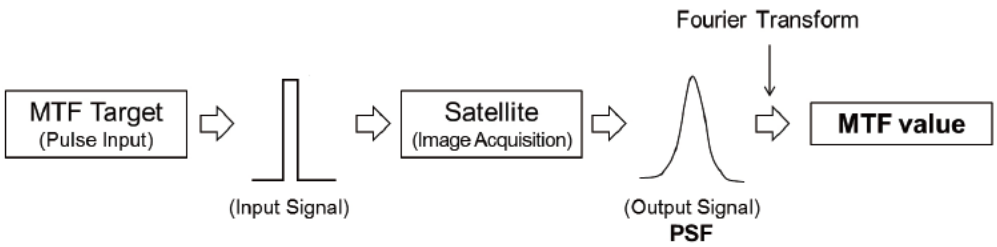

Fig. 1. Modulation transfer function (MTF) estimation process using the pulse method.

http://dx.doi.org/10.5140/JASS.2013.30.4.321

Among image restoration methods such as IF, PIF, and WF, we selected the WF method which minimizes the error in estimating the ideal image from the noisy image by linear filtering (Demoment 1989). The computational process for the WF method used in this paper is given in Eqs. (2-4):

$$g(x,y) = f(x,y) * s(x,y) + n(x,y) \tag{2}$$

$$G(u,v) = F(u,v)\, S(u,v) + N(u,v) \tag{3}$$

In Eq. (2), $g(x,y)$ is the raw image generated from the satellite, $f(x,y)$ is the diffraction limited image, and $s(x,y)$ is the PSF. Convolution computation is denoted as *, and $n(x,y)$ is the noise. The Fourier transforms of Eq. (2) are given in Eq. (3), in which the transformed functions are represented by capital letters. Eq. (4) gives the WF value in the Fourier domain:

$$\begin{aligned} W(u,v) &= \frac{S^*(u,v)}{|S(u,v)|^2 + \frac{c\Phi_N(u,v)}{\Phi_O(u,v)}} \\ &= \frac{S^*(u,v)}{|S(u,v)|^2 + \frac{1}{SNR}}, (c=1) \end{aligned} \tag{4}$$

We estimated the PSF of the target image using the WF method designed by Helstrom (1967). The WF value is denoted as $W(u,v)$ in the Fourier domain, and $\Phi_N/\Phi_{O(u,v)}$ is the ratio of the power spectrum of the noise to the object. The ratio constant, c, controls the weight of $\Phi_N/\Phi_{O(u,v)}$; we determined that c = 1 in the computational process. $\Phi_N/\Phi_{O(u,v)}$ can then be approximated by an inverse signal-to-noise ratio (SNR) (Fienup et al. 2002). In this paper, we assumed that $S(u,v)$ is PSF curve fitted by the Gaussian function constructed with σ and μ, and $\Phi_N/\Phi_{O(u,v)}$ was calculated with the image-based SNR value. Those control parameters used in Eq. (4) will be described in Section 3.

3. RESULTS

3.1 Data processing

Fig. 2 shows the regions of interest for MTF and PSF value computation (Target A) and image-based SNR (Target B). The Target A area corresponds to the Saemangeum seawall on the west coast. The MTF in this case (i.e., the complex coastline) was estimated using the pulse method. A constant signal from the East Coast area (Target B) was selected to estimate the SNR of the image and will be used as the major element of the WF. The detailed locations and sizes of the two target areas are listed in Table 2.

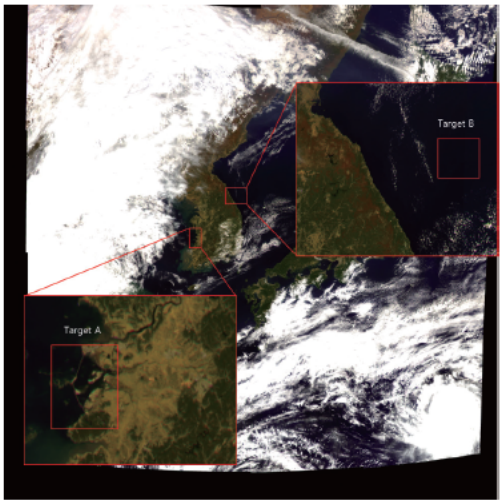

Fig. 2. Target areas. Target A and B are for calculating PSF value and SNR respectively.

Table 2. Target image areas for the modulation transfer function (MTF) and signal-to-noise (SNR) estimation.

	Target A	Target B
Latitude (°)	35.39~35.55 E	38.22°~39.20 E
Longitude (°)	126.25~126.41 N	129.93°~130.57 N

The Saemangeum seawall has an average width of 290 m, which was used to estimate the MTF value. The width of the image was estimated to be 312.02 m with a geometric slope of 67.16°. The target width as a pulse in the input signal fits the criterion of being smaller than the spatial resolution of a pixel (500 m) and is thus appropriate for our analysis. To obtain an image-based SNR, we selected an area in Target B with a chlorophyll value of less than 0.07 mg m–3. This SNR is based only on the image noise and excludes fluctuations that may exist due to ocean conditions (Hu et al. 2012).

To obtain the PSF and SNR values for the WF, the pulse signal for the target area was converted to a distribution function for each row. In Fig. 3, the radiance value for PSF for each row was ordered by the peak point at 0 pixel position (marked by 'black circular sign'). Then, the average values for the fitted curve were used to construct the PSF curve ('Red line' in Fig. 3). A Gaussian fitting curve was used to match the PSF curve as a normal distribution ('Blue line' in Fig. 3); from this, we computed σ and μ, which were 0.5645 and 0.0111, respectively. Additionally, the estimated full

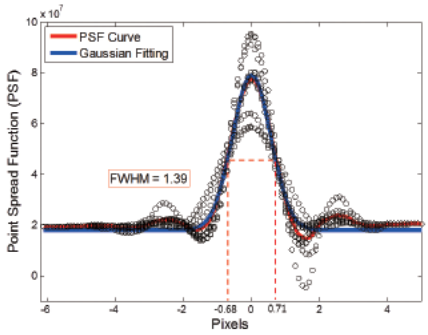

Fig. 3. Gaussian curve fitting for the estimated point spread function (PSF) from the original target image. A black circular sign means the PSF radiance value after interpolation in each pixel. Red and Blue lines are the average PSF curve and fitted Gaussian curve respectively.

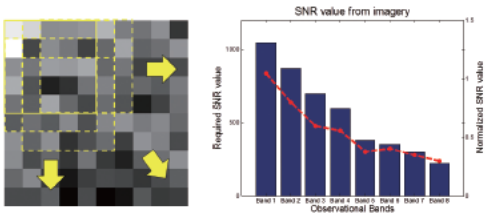

(a) SNR estimation concept (b) Estimated SNR based on the image signal at Target area 'B'

Fig. 4. The signal-to-noise (SNR) estimation concept (a) and calculated SNR value of the original image (b) for Target area 'B'.

width at half maximum (FWHM) of the fitted PSF curve was 1.3886 and did not exceed two pixels.

$$\sigma_{image}(counts) = \frac{\sum_{i=1}^{5}\sum_{j=1}^{5} DN_{ij}}{N} \quad (5)$$

$$\sigma_{image}(counts) = \frac{\sum_{i=1}^{5}\sum_{j=1}^{5} DN_{ij}}{N} \quad (6)$$

$$\sigma_{noise}(counts) = \sqrt{\frac{\sum_{i=1}^{5}\sum_{j=1}^{5} (DN_{ij} - \sigma_{image})^2}{N}} \quad (7)$$

The SNR values used in the WF for the target area (Target B) were calculated using Eq. (5) (Fig. 4). To achieve the SNR from the nearly homogeneous area in the imagery, a small square (n × n) window of pixels (in this paper, 5 × 5 pixels) was moved within the target area (100 × 100 pixels for GOCI) by one-pixel steps to obtain the average value of σ_{image} (counts) and the standard deviation value of σ_{noise} (counts), as shown in Fig. 4b.

Table 3 summarized the image restoration parameter of

Table 3. Control parameter for the MTF compensation with WF method.

Band (nm)	PSF		SNR
	σ	μ	
412	0.5645	0.0111	1045.77
443			870.36
490			698.11
555			595.48
660			379.85
680			350.87
745			299.99
865			222.14

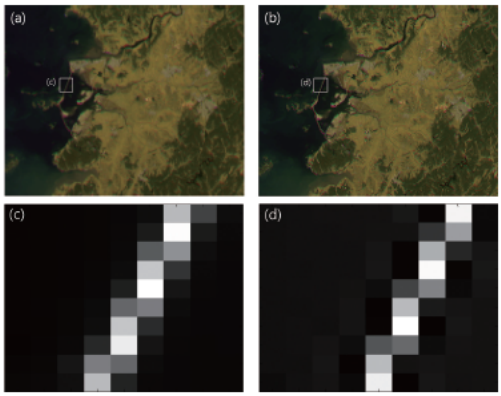

Fig. 5. (a) is the original image near Saemangum seawall, and (b) is the MTF compensated image after application of the WF. (c) and (d) image is the target area for estimating PSF value before and after application of the Wiener filter (WF) respectively.

PSF and SNR that we calculated σ and μ value of a Gaussian fitting curve at the Target area 'A', and SNR values are estimated from each band image signal of the Target area 'B'. With those parameters, we applied WF to compensate the image, and discussed the results in the Section 3.3.

3.2 Image restoration results

In Fig. 5a and b, two red-green-blue (RGB) composite image (R: 680 nm, G: 555 nm, B: 412 nm) obtained at UTC 03 on 16 October 2012 are compared that the MTF compensated image illustrates the improved image quality in aspect of sharpness and contrast in the coastal area near the Saemangeum seawall and inland river boundary. We compared the MTF results between the original and enhanced images after estimating the PSF with the WF method to confirm this difference quantitatively with using the target areas as shown in Fig. 5c and d.

The FWHM and PSF values of the reconstructed image using the WF were improved significantly compared with the original image. In Fig. 6, the FWHM and the σ

http://dx.doi.org/10.5140/JASS.2013.30.4.321

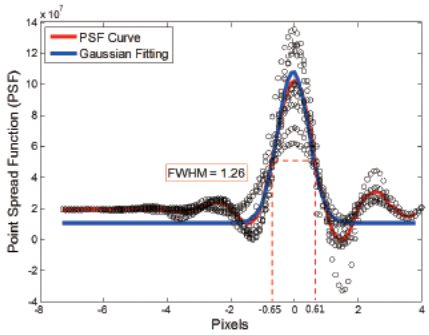

Fig. 6. Gaussian curve fitting for the estimated PSF from the enhanced target image with the WF.

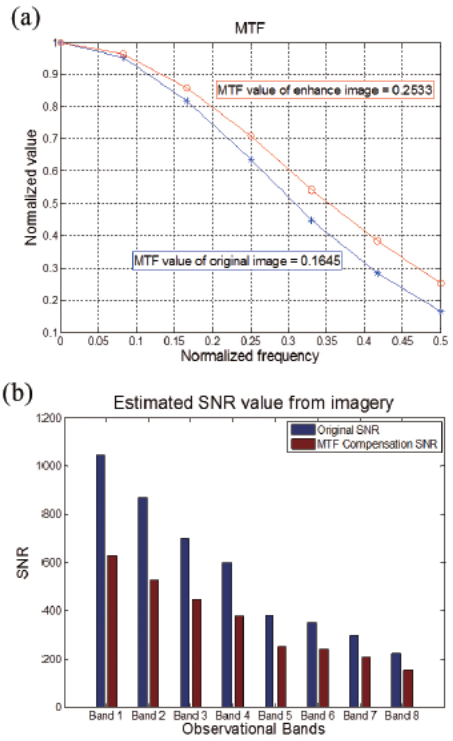

Fig. 7. (a) Comparison of MTF results between the original (blue line) and enhanced (red line) images, (b) The SNR value variation for all bands after applied WF MTF compensation.

value of the standard deviation of the Gaussian function improved from 1.3886 to 1.2600 and from 0.5645 to 0.4924, respectively. Finally, the MTF value at the Nyquist frequency increased by 35.06% (0.2533) compared with the source image as shown in Fig. 7a. On the other hand, SNR values estimated in the Target 'B' are decreased for all bands. In case of band-8, the estimated SNR value based on the image is changed from 222.14 to 155.62.

4. CONCLUDING REMARKS

This study was performed to evaluate the image quality of the GOCI system with the first suggested technique using the natural target, as well as to improve its quality with MTF compensation based on the WF method. We measured the MTF for a natural target, the Saemangeum seawall, at UTC 03 on 16 October 2012 and designed a WF with a PSF value, on the basis of MTF processing and SNR values obtained for seawater. After application of the WF to the target image, the enhanced image was generated with a 35.06% improved MTF value compared with the original image.

Despite the 500-m spatial resolution of the GOCI satellite image, it is difficult to estimate the exact PSF value. In addition, the SNR values are also relatively estimated based on the image, and that is reason why the SNR value is underestimated comparison with requirement. Although SNR value is decreased from applying MTF compensation, the enhanced image having high MTF value can be practically used in monitoring works and researches in coastal area. Furthermore, the relationship between ocean color product accuracy and MTF enhanced image will be discussed with further investigation in the near future.

Thus, the significance of this paper lies in the improvement of the image quality using the well-constructed WF method with Gaussian curve fitting. With the restoration results, the complexities of the west coast area and its islands were clearly distinguished with the naked eye as a result of the improved image quality. Additionally, this work is firstly suggested to estimate in-orbit MTF and SNR value, and generate the MTF compensated image of geostationary orbit satellite for ocean monitoring. We believe that the results of this study are expected to provide a more accurate description of the coastal regions for improvement in image processing such as cloud detection for atmospheric correction and ocean color data in coastal area.

ACKNOWLEDGMENTS

This research was a part of the project titled "Geostationary earth orbit Korea Multi-Purpose Satellite Ocean Monitoring Payload Development" funded by the Ministry of Land,

Transport and Maritime Affairs, Korea, and as Basic Research Projects (PE98985) of the Korean Institute of Ocean Science and Technology.

REFERENCES

Choi T, IKONOS Satellite on Orbit Modulation Transfer Function (MTF) Measurement using Edge and Pulse Method, MSc Thesis, South Dakota State University (2002).

Demoment G, Image reconstruction and restoration: Overview of common estimation structures and problems, Acoustics, Speech and Signal Processing, IEEE Transactions on 37, 2024-2036 (1989).

Fienup JR, Griffith DK, Harrington L, Kowalczyk A, Miller JJ, et al., Comparison of reconstruction algorithms for images from sparse-aperture systems, Proc. SPIE, 4792, 1-8 (2002).

Helstrom CW, Image restoration by the method of least squares, JOSA, 57, 297-303 (1967).

Holst GC, Electro-optical imaging system performance (SPIE press, Bellingham, Washington, 2008).

Hu C, Feng L, Lee Z, Davis CO, Mannino A, et al., Dynamic range and sensitivity requirements of satellite ocean color sensors: Learning from the past, Applied Optics, 51, 6045-6062 (2012).

Hwang H, Choi YW, Kwak S, Kim M, Park W, et al., MTF assessment of high resolution satellite images using ISO 12233 slanted-edge method, in Proc. SPIE, 7109, 710905-1-9 (2008).

Jeon B-I, Kim H, Chang YK, A MTF compensation for satellite image using L-curve-based modified Wiener filter, Korean Journal of Remote Sensing, 28, 561-571 (2012).

Jo HG, Kim JH, Choi SC, Lee SK, Kim J-M, et al., A study on the simulation method of satellite image quality considered design, manufacturing and operation, Korean Journal of Remote Sensing, 24, 591-603 (2008).

Leger D, Duffaut J, Robinet F, MTF Measurement Using Spotlight, Proc. IGARSS, 7803, 2010-2012 (1994).

Reichenbach SE, Koehler DE, Strelow DW, Restoration and reconstruction of AVHRR images, Geoscience and Remote Sensing, IEEE Transactions on 33, 997-1007 (1995).

Rojas F, Schowengerdt RA, Biggar SF, Error and correction for MODIS-AM's spatial response on the NDVI and EVI science products, Proc. SPIE, 4814, 447-456 (2002).

Ruiz CP, Lopez FJA, Restoring SPOT images using PSF-derived deconvolution filters, International Journal of Remote Sensing, 23, 2379-2391 (2002).

Ryu JH, Han HJ, Cho S, Park YJ, Ahn YH, et al., Overview of geostationary ocean color imager (GOCI) and GOCI data processing system (GDPS), Ocean Science Journal, 47, 223-233 (2012).

Smith EHB, PSF estimation by gradient descent fit to the ESF, Proc. SPIE, 6059, 60590E-1-9 (2006).

Tzannes AP, Mooney JM, Measurement of the modulation transfer function of infrared cameras, Optical Engineering, 34, 1808-1817 (1995).

Viallefont F, Edge method for on-orbit defocus assessment, Optics Express, 18, 20, 20845-20851 (2010).

Viallefont F, Leger D, Improvement of the edge method for on-orbit MTF measurement, Optics Express, 18, 4, 3531-3545 (2010).

Wu HHP, Schowengerdt RA, Improved estimation of fraction images using partial image restoration, Geoscience and Remote Sensing, IEEE Transactions on 31, 771-778 (1993).

Yin FF, Giger ML, Doi K, Measurement of the presampling modulation transfer function of film digitizers using a curve fitting technique, Medical Physics, 17, 962 (1990). http://dx.doi.org/10.1118/1.596463

Technical Paper
J. Astron. Space Sci. 31(3), 241-246 (2014)
http://dx.doi.org/10.5140/JASS.2014.31.3.241

JASS Journal of Astronomy and Space Sciences

Experimental Sensitivity Table Method for Precision Alignment of Amon-Ra Instrument

Eunsong Oh[1,2], Ki-Beom Ahn[1,2], Sug-Whan Kim[2†]

[1]Korea Ocean Satellite Center, Korea Institute of Ocean Science & Technology, Ansan P.O. Box 29, 425-600, Korea
[2]Space Optics Laboratory, Dept. of Astronomy, Yonsei University, 134 Sinchon-dong, Seodaemun-gu, Seoul, 120-749, Korea

The Amon-Ra instrument is the main optical payload of the proposed EARTHSHINE satellite. It consists of a visible wavelength instrument and an IR energy channel instrument to measure a global Earth albedo. We report a new sensitivity technique for efficient alignment of the visible channel instrument. Whilst the sensitivity table method has been widely used in the alignment process, the straightforward application of the method tends to produce slow process convergence because of shop floor alignment practice uncertainties. We investigated the error sources commonly associated with alignment practices and used them when estimating the Zernike polynomial coefficients. Aided with single center field wavefront error (WFE) measurements and their corresponding Zernike polynomial coefficients, the method involves the construction and use of an experimental, instead of simulated, sensitivity table to be used for alignment state estimations. A trial alignment experiment for the Amon Ra optical system was performed and the results show that 71.28 nm in rms WFE was achieved only after two alignment iterations. This tends to demonstrate its superior performance to the conventional method.

Keywords: Alignment, Testing, Computer-aided alignment

1. INTRODUCTION

The Albedo Monitor and Radiometer (Amon-Ra) instrument is the primary payload of the proposed EARTH-Sun-Heliosphere Interactions Experiment (EARTHSHINE) satellite (Park et al. 2007, Lee et al 2005a, 2005b). The goal of the instrument is to measure the Earth albedo variation. The instrument consists of two optical systems. The first is a visible channel instrument to observe both the Earth and Sun alternately over the wavelength range of 0.4 ~ 0.75 μm. The other is an energy channel for bolometric measurement of the incident solar and Earth reflected shortwave radiations over 0.4 ~ 4.0 μm in wavelength. The observation concept of Amon-Ra is such that it is designed to share the same optical train as much as possible, when viewing the Earth and Sun as the spacecraft rotates (Park et al. 2007, Lee et al 2005a, 2005b). Therefore, the accurate alignment of the instrument optical system is crucial for achieving the science goal. We studied the precision optical alignment of the Amon-Ra visible channel system and report the new sensitivity table alignment technique and its alignment performance in this paper.

Over the past few decades, several computer aided alignment (CAA) methods based on the Zernike polynomials have been developed to ensure the efficient alignment of optical systems (Jeong et al. 1987, Rimmer 1990, Chapman & Sweeney 1998, Zhang et al. 2000, Kim et al. 2007, Lee et al 2007). Among them, the sensitivity table technique is arguably the most widely used method to align two-mirror and three-mirror systems (Jeong et al. 1987, Rimmer 1990, Chapman & Sweeney 1998, Zhang et al. 2000, Kim et al. 2007, Bin et al. 2010, Kea et al. 2008, Zhao et al. 2010, Kim et al. 2005, Yang et al. 2004).

Received Jun 2, 2014 **Revised** Sep 3, 2014 **Accepted** Sep 4, 2014
†**Corresponding Author**
E-mail: skim@csa.yonsei.ac.kr
Tel: +82 2 362 7891, Fax: +82-2-362-7891

http://janss.kr pISSN: 2093-5587 eISSN: 2093-1409

$$\begin{bmatrix} Z_{11} \\ \vdots \\ Z_{m1} \end{bmatrix} = \begin{bmatrix} A_{11} & \cdots & A_{n1} \\ \vdots & \ddots & \vdots \\ A_{1n} & \cdots & A_{mn} \end{bmatrix} \begin{bmatrix} D_{11} \\ \vdots \\ D_{1n} \end{bmatrix} \quad (1)$$

The technique uses Eq. 1, where $[Z_{11}, \cdots, Z_{m1}]$ form the Zernike polynomials representing the measured system wavefront errors (WFE) at the arbitrary alignment state. The D matrix describes the alignment deviation of the optical element parameters, such as decenter and tilt, from those of the ideal alignment state. $[A_{11}, \cdots, A_{mn}]$ form the Zernike sensitivity table constructed from changes in Zernike coefficients corresponding to alignment parameter variations.

$$A_{mn} = \frac{\Delta Z_m}{\Delta D_n} \quad (2)$$

Typically, Eq. 2 is required to build a sensitivity table (A_{mn}), where ΔZ_m represents the changes in the Zernike coefficient caused by variations in the alignment parameters (ΔD_n) such as decenter and tilt. The conventional method used to obtain A_{mn} is to compute ΔZ_m while adjusting ΔD_n in ray tracing simulation using software such as Code V and ZEMAX.

However, it is well known that resulting A_{mn} tends to produce its nonlinearity to ΔD_n and it needs lengthy multi-field measurements to improve the estimation accuracy of ΔZ_m (Kim et al. 2007, Kim et al. 2009, Oh et al. 2010). In addition, the technique also tends to ignore measurement field pointing uncertainties, apparatus control uncertainties, and part surface form accuracy. These contribute to increasing differences between simulated and measured Zernike coefficients $[Z_{11}, \cdots, Z_{m1}]$ and their variations ΔZ_m and, therefore, the resulting sensitivity table A_{mn}.

In this paper, we improve the technique with a simple and practical conceptual shift to the use of experimental sensitivity table, being away from the simulated one. Section 2 describes the theoretical method, the target optical system characteristics used and the application of the new experimental sensitivity table method. Alignment simulations and experimental results are described in Section 3, demonstrating its superior performance to that of the conventional method. In Section 4, the implications of the new experimental sensitivity method are summarized.

2. NEW EXPERIMENTAL SENSITIVITY METHOD

2.1 Theoretical method

The experimental sensitivity table can be constructed by replacing the simulated A_{mn} with the experimental A_{mn} obtained from multiple center field, as opposed to multi-field, WFE measurements (ΔZ_m) while the alignment parameters associated with each optical component are changed in known steps ΔS_n, as in Eq. 3. In this way, the experimental sensitivity table is built while reflecting the sum of all aforementioned uncertainties.

$$A_{mn} = \frac{\Delta Z_m}{\Delta S_n} \quad (3)$$

Once it has been built, solving Eq.1 requires for an inverse matrix A^+_{mn} of A_{mn}. The singular value decomposition (SVD) was used to derive A^+_{mn} as in Eq.4, where $D_{3\times1}$ means the deviations of the alignment parameter such as Decenter X, Decenter Y, and Tilt Y in this study. $Z_{4\times1}$ is fringe Zernike coefficients from the 5th to the 8th term when measuring at the center field. For the alignment case study described in Section 2.2, SVD of an 4×3 matrix A is transformed to the inverse matrix (A^+) consisting of three matrix. U^T is an 4×4 unitary matrix, V is an 3×3 unitary matrix, and Σ^+ is an 4×3 diagonal matrix having singular values of A in the diagonal entries (Σ^+_{11} : 2.9009, Σ^+_{22} : 0.0341, Σ^+_{33} : 0.0016). We then computed and traced the alignment state of the optical system for each step alignment experiment.

$$D_{3\times1} = A^+ Z_{4\times1}$$
$$A^+ = V \Sigma^+ U^T \quad (4)$$

2.2 Target optical system: Two-mirror system with high obscuration

To experimentally verify the performance increase resulting from such a simple yet practical conceptual shift, we used a catadioptric optical system of high obscuration from the relatively large secondary mirror of 38 mm in diameter as shown in Table 1. Its optical system consists of two mirrors and four corrector lenses. Incident light rays are reflected from the system's primary mirror (M1) that is 76 mm in diameter and -1.0 in conic constant, and then from its secondary mirror (M2). The M2 alignment tolerance was computed to ± 140.0 μm in decenter and ± 100.0 arcsec in tilt (Fig. 1-(a)). The system alignment was required to meet the requirement of 126.56 nm in rms WFE (Lee et al. 2005b). The alignment test configuration has the target optical system sandwiched in between a phase-shifting interferometer and a reference flat mirror, as shown in Fig. 1. M1 and the corrector lens barrel were already aligned and fixed to each other via the M1 support plate within the predetermined tolerance level. The despace between

Table 1. Measured specification of optical elements of target optical system (Park et al. 2007).

No.	Optical Elements	Radius of curvature[b]	Diameter(mm)	Glass
1	Primary Mirrora	-290.39	76.00	Mirror
2	Secondary Mirror	-273.38	38.00	Mirror
3	Corrector Lens 1	104.37 (F)	29.00	F-Silica
4		40.03 (R)	29.00	
5	Corrector Lens 2	89.95 (F)	28.99	CaF2
6		-49.53 (R)	28.99	
7	Corrector Lens 3	22.92 (F)	24.99	F-Silica
8		18.91 (R)	24.99	
9	Corrector Lens 4	-28.08 (F)	24.99	F-Silica
10		-34.07 (R)	24.99	

a Conic Constant of Primary Mirror is -1.0, and other elements are spherical (conic =0.0).
b (F) means a front surface, and (R) is a rear surface of lens respectively.

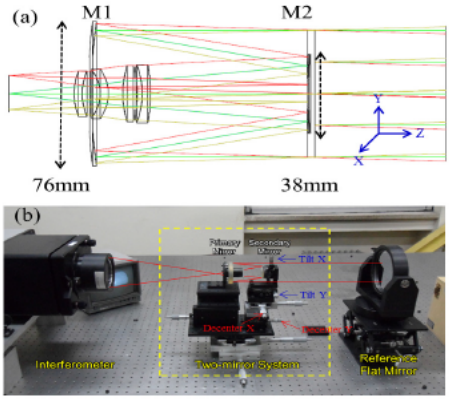

Fig. 1. (a) 2-D layout of Amon-Ra, (b) Alignment set-up environment.

M1 and M2 was also aligned for the minimum spherical aberration value so that it was not regarded as the alignment parameter that can affected by the lens barrel states. M2 decenter and tilt are the two alignment variables that need to be controlled in order to achieve alignment, and this paper is focusing at the M2 precise alignment.

Table 2. Sensitivity table from the conventional simulation and from this experiment using M2 (i.e., on-axis center field measurement only).

	Zernike Coefficient	Decenter X	Decenter Y	Tilt X	Tilt Y
Conventional simulation method	Term 5	3.98×10^{-10}	-2.97×10^{-10}	1.42×10^{-10}	2.68×10^{-10}
	Term 6	-2.59×10^{-10}	-2.79×10^{-10}	3.50×10^{-11}	1.60×10^{-12}
	Term 7	-5.03×10^{-1}	1.12×10^{-8}	-1.32×10^{-9}	2.40
	Term 8	9.92×10^{-9}	-5.03×10^{-1}	-2.40	3.05×10^{-9}
New experimental method	Term 5	0.0008	0.0046	Nan	-0.7106
	Term 6	-0.0094	0.0000	Nan	1.1304
	Term 7	-0.0282	0.0095	Nan	1.7050
	Term 8	-0.0602	0.0262	Nan	1.9291

2.3 Simulations and experiments with experimental sensitivity table method

First, the experimental sensitivity table was constructed from a series of wavefront measurement at the center field. From the approximated alignment status, M2 was moved 5 μm for decenter and 0.18 arcmin for tilt in a sampling step. The system WFE was then measured, and its corresponding Zernike polynomial coefficients were obtained three times at each measurement location for decenter and tilt for x and y axes, respectively. The resulting Zernike coefficient variation trends for the y-axis tilt are shown in Fig. 2 as an example.

Once all the measurements were completed, we then polynomial-fit the Zernike coefficient variation over the decenter and tilt ranges used. In the polynomial fitting, we used the linear fitting equation which is the same process with Eq. 1. and 2. The final sensitivity table was then constructed, as shown in Table 2 where the resulting sensitivities from both conventional and experimental methods are compared. We note that the experiment to determine Zernike coefficients for x axis tilt was not performed because of the inaccurate goniometer tilt X motion caused by its unpredictable backlash characteristics.

The fringe Zernike coefficients from the 5th to the 8th term representing high order aberrations are listed in Table 2. In general, the 7th term Zernike coefficient is closely

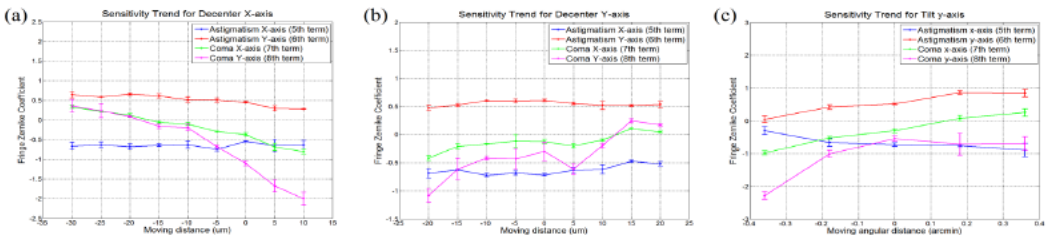

Fig. 2. Fringe Zernike sensitivity variations when (a) decentering to x-axis, (b) decentering to y-axis, and (c) tilting to y-axis tilt parameter of M2.

Table 3. Calculated inverse matrix (A^+) of using SVD technique from the sensitivity table in Table 2.

	Zernike Coefficient	Decenter X	Decenter Y	Tilt Y
Conventional simulation method	Term 5	4.64×10^{-10}	-1.12×10^{-11}	-2.82×10^{-10}
	Term 6	-2.97×10^{-10}	-2.79×10^{-10}	-1.42×10^{-09}
	Term 7	4.37×10^{-1}	-2.49×10^{-1}	2.09
	Term 8	2.49×10^{-1}	4.37×10^{-1}	1.19
New experimental method	Term 5	0.0159	-0.6130	0.3590
	Term 6	0.0309	-1.2519	0.7455
	Term 7	0.0439	-1.8358	1.1243
	Term 8	-0.0230	0.9013	-0.5819

related to the x-axis decenter and the y-axis tilt, while the 8th term is sensitive to the y-axis decenter and the x-axis tilt. From Table 1, it is clear that the y-axis tilt plays the most significant role in the Zernike coefficients' sensitivity.

The conventional method shows ~$10^{-10\sim-12}$ in the 5th and 6th term Zernike coefficients, illustrating the negligible effects of decenter and tilt variations on the on-axis field measurement. We note that, whilst their magnitude is somewhat smaller than the others, the 7th and 8th term coefficients also show increasing sensitivity trends similar to those of the 5th and 6th terms as well. These prove that the aforementioned measurement field positioning and apparatus control error significantly influence the resulting sensitivities.

Second, using the sensitivities in Table 2 and Eq. 4, we computed and compared the inverse sensitivity tables (A^+) between the conventional simulation method and the new experimental method. With these inverse matrixes of sensitivity table, we performed two simulations and one experiment that is described in section 3.

3. ALIGNMENT SIMULATION AND EXPERIMENT RESULTS

Fig. 3 shows the results from two alignment simulations and one experiment. Fig. 3-(a) illustrates the results from using the target optical system design without any additional errors included. We note that, in this ideal case, both conventional and experimental sensitivity methods are capable of producing the alignment state estimation (i.e., solution) after the first iteration.

The results in Fig. 3-(b) were obtained with 82.264 nm rms WFE in surface fabrication error introduced to M2. Both methods show similar performance in decreasing the simulated system wavefront below the requirement, although the experimental sensitivity method shows marginally better estimation after the 1st iteration.

The results of the real alignment experiment appear in Fig. 3-(c). The conventional method shows an alignment divergence, even for the 1st alignment correction, which was caused by an incorrect estimation of Zernike fringe coefficients. On the other hand, the experimental sensitivity table method estimated the alignment state accurately and is capable of reducing the system's wavefront to make it lower than the requirement in just two iterative alignment actions.

In Fig. 4 and Table 4, he initial alignment state at the center field is 362.71 nm rms WFE, where the new method's estimate for the system's misalignment is 0.0395 mm in the x-axis decenter, -0.0124 mm in the y-axis decenter, and -2.5472 arcmin in the y-axis tilt parameter. We adjusted the M2 location by the same amounts but to the opposite direction from the misalignment computed above. Then the alignment state improved to 192.15 nm rms WFE. After iterating one more similar alignment action with using Table 4, the optical system rms WFE became 71.28 nm in the on-axis field, excluding the masked area, which is better than the requirement, as shown in Fig. 4.

4. CONCLUDING REMARKS

We performed the alignment experiment for the visible channel optical system of Amon-Ra instrument successfully

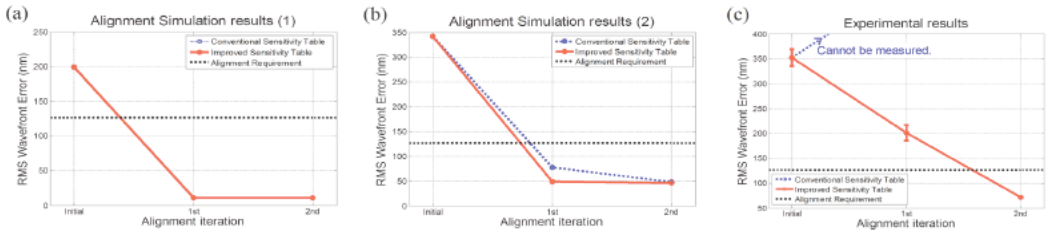

Fig. 3. Alignment performance results from two methods (blue dotted line : conventional sensitivity table, red line : experimental sensitivity table). (a) is the simulation results for the the optical system without fabrication error. (b) is the simulation results for the de designed optical system with surface fabrication WFE errors included and (c) is resulted from the actual alignment experiment.

http://dx.doi.org/10.5140/JASS.2014.31.3.241

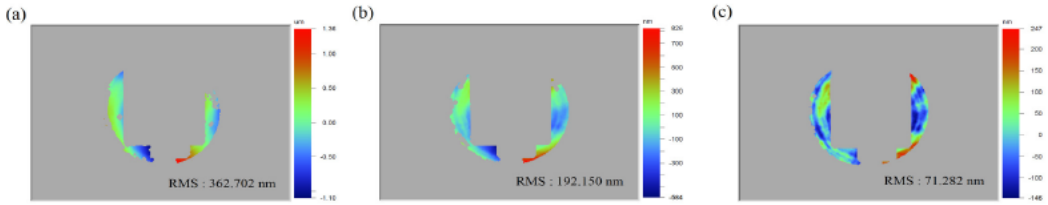

Fig. 4. Evolution of the WFE map after the experimental sensitivity table method shown in Fig. 3-(c) was used. (a) shows WFE map of the initial misaligned state, (b) was obtained after 1st alignment iteration, and (c) is the final WFE map after 2nd alignment iteration.

Table 4. The measurement results of alignment state using the experimental sensitivity table.

Iterations		Initial state	1st aligned state	2nd aligned state
Measured Zernike coefficients	Term 5	3.29×10^{-2}	-8.27×10^{-1}	-1.05×10^{-1}
	Term 6	-3.28×10^{-1}	-2.28×10^{-1}	4.09×10^{-2}
	Term 7	-1.4593	1.26×10^{-1}	2.03×10^{-1}
	Term 8	-2.8734	-1.3163	-2.08×10^{-1}
Adjusted alignment parameters	Decenter X	-	0.0395	-0.0086
	Decenter Y	-	-0.0124	-0.0012
	Tilt Y	-	-2.5472	1.0798
RMS wavefront error (nm)		362.702	192.150	71.282

using the new experimental sensitivity table method. The resulting optical alignment performances between the conventional and the new technique are compared. In summary, the target optical system has technical difficulty when measuring a wavefront map because of the high obscuration (of 79.40%) caused by M2 (Park et al. 2007) and the support structure. The conventional (i.e., simulated sensitivity from the optical design) method produces an incorrect estimation of its alignment state in real experiments, largely due to the measurement uncertainties. On the other hand, the new and improved (i.e., experimentally obtained sensitivity with the on-axis center field measurement) method is capable of satisfying the WFE requirement in just two alignment actions. This proves that the experimental sensitivity method studied here would offer considerable efficiency and accuracy to the shop floor alignment process with its simplicity and high degree of practicality.

ACKNOWLEDGEMENTS

This work is supported by "Geostationary earth orbit Korea Multi-Purpose Satellite Ocean Monitoring Payload Development" funded by the Ministry of Land, Transport and Maritime Affairs of Korean government and "Optical Performance Simulation of Geostationary Ocean Color Imager" (PE99241) of the Korea Institute Ocean Science and Technology. The manuscript preparation is also supported in part by SRC program (2010-0027910) from Center for Galaxy Evolution Research (CGER). This research was also supported by the Korea Astronomy and Space Science Institute under the R&D program (Project No. 2014-9-710-03) supervised by the Ministry of Science, ICT and Future Planning.

REFERENCES

Bin W, Lei JS, Tian Q, Study on computer-aided alignment method of Cassegrain system, SPIE 7654, 765405 (2010). http://dx.doi.org/10.1117/12.867978

Chapman HN, Sweeney DW, Rigorous method for compensation selection and alignment of microlithographic optical systems, SPIE 3331, 102-113 (1998). http://dx.doi.org/10.1117/12.309562

Jeong HJ, Lawrence GN, Nahm KB, Auto-alignment of a three mirror off-axis telescope by reverse optimization and end-to-end aberration measurements, SPIE 0818, 419-430 (1987). http://dx.doi.org/10.1117/12.978915

Kea L, Yanqiu L, Jingfenga L, Cuifangb K, Computer aided alignment of a 20X Schwarzschild projection optics, SPIE 7130, 713042 (2008). http://dx.doi.org/10.1117/12.819705

Kim ED, Choi YW, Kang MS, Choi SC, Reverse-optimization Alignment Algorithm using Zernike Sensitivity, JOSK 9, 68-73 (2005).

Kim S, Yang HS, Lee YW, Kim SW, Merit function regression method for efficient alignment control of two-mirror optical systems, OExpr 15, 5059-5068 (2007). http://dx.doi.org/10.1364/OE.15.005059

Kim Y, Yang HS, Kim SW, Lee YW, Alignment of off-axis optical system with multi mirrors using derivative of Zernike polynomial coefficient, SPIE 7433, 74330C (2009). http://dx.doi.org/10.1117/12.825826

Lee H, Dalton GB, Tosh IAJ, Kim SW, Computer-guided alignment II: Optical system alignment using differential wavefront sampling, OExpr 15, 15424-15437 (2007). http://dx.doi.org/10.1364/OE.15.015424

Lee H, Kim SW, Richards T, Tosh I, Morris N, et al., Stray-light analysis of Amon-Ra instrument, SPIE 5867, 46-57 (2005a). http://dx.doi.org/10.1117/12.639585

Lee H, Tosh I, Morris N, Lockwood M, Kim SW, The optomechanical design of Amon-Ra instrument, SPIE 5638, 248-261 (2005b). http://dx.doi.org/10.1117/12.573624

Oh ES, Kim S, Kim Y, Lee H, Kim SW, et al., Integration of differential wavefront sampling with merit function regression for efficient alignment of three-mirror anastigmat optical system, SPIE 7793, 77930F (2010). http://dx.doi.org/10.1117/12.860767

Park WH, Kim S, Lee H, Yi HS, Lee JM, et al., Optical Performance of Breadboard Amon-Ra Imaging Channel Instrument for Deep Space Albedo Measurement, JASS 24, 79-90 (2007). http://dx.doi.org/10.5140/JASS.2007.24.1.079

Rimmer MP, A computer aided optical alignment method, SPIE 1271, 363-368 (1990). http://dx.doi.org/10.1117/12.20423

Yang HS, Lee YW, Kim ED, Choi YW, Rasheed AAA, Alignment methods for Cassegrain and RC telescope with wide-field of view, SPIE 5528, 334-341 (2004). http://dx.doi.org/10.1117/12.558998

Zhang B, Zhang X, Wang C, Han C, Computer-aided alignment of the complex optical system, SPIE 4231, 67-72 (2000). http://dx.doi.org/10.1117/12.402830

Zhao X, Jiao W, Liao Z, Wang Y, Chen J., Study on computer-aided alignment method of a three-mirror off-axis aspherical optical system, SPIE 7656, 76566M (2010). http://dx.doi.org/10.1117/12.865582

GOCI image enhancement using an MTF compensation technique for coastal water applications

Eunsong Oh[1,2] and Jong-Kuk Choi[1,*]

[1]*Korea Ocean Satellite Center, Korea Institute of Ocean Science and Technology, 787 Haeanro, Ansan 426-744, South Korea*

[2]*Space Optics Laboratory, Dept. of Astronomy, Yonsei University, 134 Sinchon-dong, Seodaemun-gu, Seoul 120-749, South Korea*

jkchoi@kiost.ac

Abstract: The Geostationary Ocean Color Imager (GOCI) is the first optical sensor in geostationary orbit for monitoring the ocean environment around the Korean Peninsula. This paper discusses on-orbit modulation transfer function (MTF) estimation with the pulse-source method and its compensation results for the GOCI. Additionally, by analyzing the relationship between the MTF compensation effect and the accuracy of the secondary ocean product, we confirmed the optimal MTF compensation parameter for enhancing image quality without variation in the accuracy. In this study, MTF assessment was performed using a natural target because the GOCI system has a spatial resolution of 500 m. For MTF compensation with the Wiener filter, we fitted a point spread function with a Gaussian curve controlled by a standard deviation value (σ). After a parametric analysis for finding the optimal degradation model, the σ value of 0.4 was determined to be an optimal indicator. Finally, the MTF value was enhanced from 0.1645 to 0.2152 without degradation of the accuracy of the ocean color product. Enhanced GOCI images by MTF compensation are expected to recognize small-scale ocean products in coastal areas with sharpened geometric performance.

OCIS codes: (010.0280) Remote sensing and sensors; (100.2980) Image enhancement.

References and links

1. J.-H. Ryu, H.-J. Han, S. Cho, Y.-J. Park, and Y.-H. Ahn, "Overview of geostationary ocean color imager (GOCI) and GOCI data processing system (GDPS)," Ocean Sci. J. **47**(3), 223–233 (2012).
2. J.-K. Choi, Y. J. Park, J. H. Ahn, H.-S. Lim, J. Eom, and J.-H. Ryu, "GOCI, the world's first geostationary ocean color observation satellite, for the monitoring of temporal variability in coastal water turbidity," J. Geophys. Res. **117**, C09004 (2012).
3. J.-K. Choi, Y. J. Park, B. R. Lee, J. Eom, J.-E. Moon, and J.-H. Ryu, "Application of the Geostationary Ocean Color Imager (GOCI) to mapping the temporal dynamics of coastal water turbidity," Remote Sens. Environ. **146**, 24–35 (2014).
4. H. Yang, J. K. Choi, Y. J. Park, H. J. Han, and J. H. Ryu, "Application of the Geostationary Ocean Color Imager (GOCI) to estimates of ocean surface currents," J. Geophys. Res. Oceans **119**(6), 3988–4000 (2014).
5. X. He, Y. Bai, D. Pan, N. Huang, X. Dong, J. Chen, C.-T. A. Chen, and Q. Cui, "Using geostationary satellite ocean color data to map the diurnal dynamics of suspended particulate matter in coastal waters," Remote Sens. Environ. **133**, 225–239 (2013).
6. X. Lou and C. Hu, "Diurnal changes of a harmful algal bloom in the East China Sea: Observations from GOCI," Remote Sens. Environ. **140**, 562–572 (2014).
7. C. Hu, L. Feng, Z. Lee, C. O. Davis, A. Mannino, C. R. McClain, and B. A. Franz, "Dynamic range and sensitivity requirements of satellite ocean color sensors: learning from the past," Appl. Opt. **51**(25), 6045–6062 (2012).
8. C. Hu, L. Feng, and Z. Lee, "Evaluation of GOCI sensitivity for at-sensor radiance and GDPS-retrieved chlorophyll-a products," Ocean Sci. J. **47**(3), 279–285 (2012).

#220807 - $15.00 USD Received 27 Aug 2014; revised 28 Sep 2014; accepted 11 Oct 2014; published 22 Oct 2014

9. D. Leger, J. Duffaut, and F. Robinet, "MTF measurement using spotlight," in *Proceedings of IGARSS. Surface and Atmospheric Remote Sensing: Technologies, Data Analysis and Interpretation* (IEEE, 1994), pp. 2010–2012.
10. D. Leger, F. Viallefont, E. Hillairet, and A. Meygret, "In-flight refocusing and MTF assessment of SPOT5 HRG and HRS cameras," Proc. SPIE **4881**, 224–231 (2003).
11. G. C. Holst, *Electro-Optical Imaging System Performance* (SPIE-International Society for Optical Engineering, 2008)
12. F. Viallefont-Robinet and D. Léger, "Improvement of the edge method for on-orbit MTF measurement," Opt. Express **18**(4), 3531–3545 (2010).
13. T. Choi, "IKONOS satellite on orbit modulation transfer function (MTF) measurement using edge and pulse method," MSc Thesis, south Dakota State University (2002).
14. M. K. Cook, B. A. Peterson, G. Dial, L. Gibson, F. W. Gerlach, K. S. Hutchins, R. Kudola, and H. S. Bowen, "IKONOS technical performance assessment," Proc. SPIE **4381**, 94–108 (2001).
15. M. Crespi and L. De Vendictis, "A procedure for high resolution satellite imagery quality assessment," Sensors 9(5), 3289–3313 (2009).
16. Z. Wang, T. Choi, and X. Xiong, "On-orbit modulation transfer function characterization of terra MODIS using the moon," Proc. SPIE **8153**, 81531N (2011).
17. T. J. Choi, N. Che, and X. J. Xiong, "On-orbit aqua MODIS modulation transfer function trending in along-scan from the Spectro-Radiometric Calibration Assembly," Proc. SPIE **7081**, 70810A (2008).
18. Z. Wang and X. Xiong, "VIIRS on-orbit spatial characterization using the Moon," IEEE Geosci. Remote Sens. Lett. **11**(6), 1116–1120 (2013).
19. E. Oh, S.-W. Kim, S.-I. Cho, J.-H. Ryu, and Y.-H. Ahn, "Initial on-orbit modulation transfer function performance analysis for Geostationary Ocean Color Imager," J. Astron. Space Sci. **29**(2), 199–208 (2012).
20. E. Oh, K.-B. Ahn, S. Cho, and J.-H. Ryu, "A modulation transfer function compensation for the Geostationary Ocean Color Imager (GOCI) based on the wiener filter," J. Astron. Space Sci. **30**(4), 321–326 (2013).
21. W. Hou, D. J. Gray, A. D. Weidemann, G. R. Fournier, and J. Forand, "Automated underwater image restoration and retrieval of related optical properties," in *Proceedings of IGARSS* (IEEE, 2007), pp. 1889–1892.
22. W. Hou, A. D. Weidemann, D. J. Gray, and G. R. Fournier, "Imagery-derived modulation transfer function and its applications for underwater imaging," Proc. SPIE **6696**, 669622 (2007).
23. W. Hou, D. J. Gray, A. D. Weidemann, and R. A. Arnone, "Comparison and validation of point spread models for imaging in natural waters," Opt. Express **16**(13), 9958–9965 (2008).
24. X. Li, X. Gu, T. Yu, T. Cheng, J. Li, H. Gao, and Z. Wang, "Atmospheric scattering and turbulence modulation transfer function for CCD cameras on CBERS-02b and HJ-1A/1B," Int. J. Remote Sens. **33**(7), 2130–2151 (2012).
25. X. Li, X. Gu, Q. Fu, T. Yu, H. Gao, J. Li, and L. Liu, "Removing atmospheric MTF and establishing an MTF compensation filter for the HJ-1A CCD camera," Int. J. Remote Sens. **34**(4), 1413–1427 (2013).
26. Y.-K. Choi and J.-N. Kwon, "Seasonal variation of transparency in the Southeastern Yellow Sea," J. Korean Fish. Soc **31**, 323–329 (1998).
27. B. Lee, J. H. Ahn, Y.-J. Park, and S.-W. Kim, "Turbid water atmospheric correction for GOCI: Modification of MUMM algorithm," Korean J. Remote Sens. **29**(2), 173–182 (2013).
28. K. G. Ruddick, F. Ovidio, and M. Rijkeboer, "Atmospheric correction of SeaWiFS imagery for turbid coastal and inland waters," Appl. Opt. **39**(6), 897–912 (2000).
29. C. D. Mobley, "Estimation of the remote-sensing reflectance from above-surface measurements," Appl. Opt. **38**(36), 7442–7455 (1999).
30. J. C. Storey, "Landsat 7 on-orbit modulation transfer function estimation," Proc. SPIE **4540**, 50–61 (2001).
31. E. H. B. Smith, "PSF estimation by gradient descent fit to the ESF," Proc. SPIE **6059**, 60590E (2006).
32. R. C. Gonzalez, *Digital Image Processing Using MATLAB*, 2nd ed. (McGraw-Hill, 2002).
33. C. W. Helstrom, "Image restoration by the method of least squares," J. Opt. Soc. Am. **57**(3), 297–303 (1967).
34. J. R. Fienup, D. K. Griffith, L. Harrington, A. Kowalczyk, J. J. Miller, and J. A. Mooney, "Comparison of reconstruction algorithms for images from sparse-aperture systems," Proc. SPIE **4792**, 1–8 (2002).

1. Introduction

The Geostationary Ocean Color Imager (GOCI), the world's first geostationary ocean remote-sensing instrument, was successfully launched on 27 June 2010 to monitor short-term variability in the ocean environment. The GOCI provides eight images per day during daytime at hourly intervals around the northeast Asian region and can be applied to a variety of studies, such as suspended sediment and chlorophyll-*a* (Chl-*a*) concentration monitoring. The GOCI covers an area of 2500 × 2500 km centered at 36°N, 130°E, with 16 slots and a 500 m spatial resolution [1]. The GOCI provides near-real-time ocean products such as water-leaving radiance (L_w), Chl-*a*, total suspended sediments (TSSs), and colored dissolved organic matter (CDOM) [1]. Recently, some studies on temporal variations in coastal waters have been carried out using the advantage of GOCI's high-frequency image acquisition [2–6].

#220807 - $15.00 USD Received 27 Aug 2014; revised 28 Sep 2014; accepted 11 Oct 2014; published 22 Oct 2014

However, the relatively low spatial resolution of the GOCI leads to a limitation in monitoring the coastal environment in detail, particularly in areas having complex geomorphological features such as the west coast of the Korean Peninsula. To mitigate this limitation, high optical performance is important and should be monitored continuously and precisely. The principal parameters indicating the optical performance of the ocean color sensor are the signal-to-noise ratio (SNR) and modulation transfer function (MTF). The SNR is widely used for estimating radiometric performance to observe small changes in ocean properties [7, 8]. In addition, the MTF value, the focus of the present paper, has been generally used as a barometer to estimate the sensor's spatial performance and it can be by several parameters, including launching vibration effects, blurring of the atmosphere, and image motion from jitter of the satellite or movement of the spacecraft during image acquisition [9–12].

On-orbit MTF assessments to monitor the sensor's spatial performance and long-term degradation have been attempted in various cases with different measurement techniques. In the case of high spatial resolution satellite images such as those of IKONOS, OrbView, and Satellite Pour l'Observation de la Terre (SPOT), the on-orbit MTF is usually calculated with the knife-edge and pulsed-source methods based on a well-contrasted artificial target [12–15]. However, low spatial resolution remote-sensing images such as those of the Moderate Resolution Imaging Spectroradiometer (MODIS) and Visible Infrared Imager Radiometer Suite (VIIRS) have generally relied on an edge spread function of the moon rather than an artificial target on the ground [16–18]. Also, to estimate GOCI's spatial performance, Oh et al. used the coastline of the East Sea and an isolated island of the South Sea in the Korean Peninsula as well as a seawall to apply an artificial target [19, 20].

Other MTF studies for remote-sensing sensors have considered image restoration and compensation with the shape and amount of its value. For example, because the MTF is strongly related to ocean surface conditions and the optical properties of the water surface, its variability and correlation have been studied. Underwater image restorations have been approached to estimate the scattering properties for water images with conventional decomposition, such as the Wiener, Lucy–Richardson, and blind deconvolutions [21–23]. Also, atmospheric MTF estimation and compensation research has been performed to enhance the radiometric response performance of high-resolution satellite sensors such as CBERS-02b and HJ-1A/1B [24, 25].

These studies to assess MTF values were focused mainly on optical performance estimation of the sensor, and compensations related to image sharpness and visibility were aimed mainly at improving image quality and more clearly distinguishing the desired results for a specific application. However, an excessive MTF compensation can occasionally affect the original including the raw image, which leads to contaminated application results. Furthermore, before this research, attempt had rarely been analyzed the relationship of MTF with ocean application results of GOCI. Therefore, we report mainly about the MTF value characterization as a geometric performance of GOCI and image quality enhancement by using MTF deconvolution based on the Wiener filter (WF). In addition, we first suggest the optimal point spread function (PSF) value to compensate the remotely sensed image without varying the original ocean color data for the GOCI.

#220807 - $15.00 USD Received 27 Aug 2014; revised 28 Sep 2014; accepted 11 Oct 2014; published 22 Oct 2014

3 November 2014 | Vol. 22, No. 22 | DOI:10.1364/OE.22.026908 | OPTICS EXPRESS 26910

2. Data and methods

2.1. Data: GOCI image and in situ measurement data

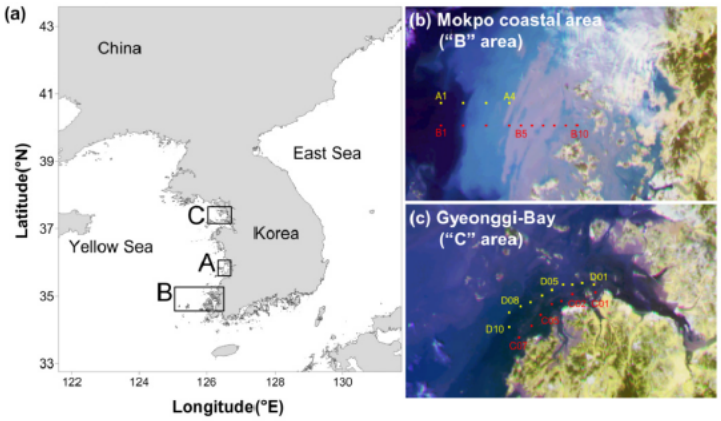

Fig. 1. (a) Location of the study area with the Saemangum area (marked in A) for estimating the MTF value with the natural-pulsed source target, (b) 14 stations in the Mokpo area (area B) for assessing the accuracy of the ocean color product using in situ measurement data acquired on 16 October 2012, and (c) 17 stations in Gyeonggi Bay acquired on 11 June 2011 for verifying the Mokpo area result from the MTF compensation.

We selected GOCI images acquired on 16 October 2012 and obtained a total of 56 images, six times (from 09:15 to 15:45) for eight band images. For the LT 16:15 and 17:15 image data, we could not analyze the data because the target area was covered by clouds and because the acquisition mission schedule was cancelled by the GOCI satellite station keeping mode, respectively. For these images, the Saemangeum seawall [marked "A" in Fig. 1] was selected as a natural MTF target area. Different from other high-resolution satellites using a human-made MTF target on the ground, finding a long and narrow artificial target was the best way to use the pulse or slant-edge method, as the spatial resolution of GOCI is 500 m. The Saemangeum seawall was the best MTF target because it has an average width of 290 m; the width in the image was estimated to be 312.02 m with a geometric slope of 67.16°. Another study area [marked "B" in Fig. 1] for comparison with ocean product accuracy was the south-western coastal area of the Korean Peninsula (hereafter, Mokpo coastal area). The Mokpo coastal area is a sensitive region having a complex coastline and turbid water. Because the Mokpo coastal area has a high suspended sediment concentration with an average of more than 20 g/m^3, its environment can affect MTF estimation significantly [26]. A third study area for verification of MTF compensation sensitivity was Gyeonggi Bay [marked "C" in Fig. 1], which is characterized by shallow and turbid water, and is thus well suited to be a verification target of the image-processing result of the Mokpo coastal area. In addition, we used in situ measurement data and GOCI images acquired on 11 June 2011 (total of 56 images for the eight bands).

Image processing was started from L1B GOCI data for all bands, and those data had already been processed by radiometric and geometric correction. Then, we performed atmospheric correction to calculate the ocean product and compare with a quantitative value such as the remote-sensing reflectance (Rrs) or normalized water-leaving radiance (nL_w), with the modified Management Unit of the North Sea Mathematical Model (MUMM) algorithm [27, 28]. The modified MUMM algorithm used in this paper, especially important near the

#220807 - $15.00 USD Received 27 Aug 2014; revised 28 Sep 2014; accepted 11 Oct 2014; published 22 Oct 2014

Korean Peninsula coastal region having high turbidity, is different from the conventional MUMM in that it can alter the α parameter iteratively to contain an optimal factor (α value) at each pixel [27].

Table 1. Relationship between In Situ Measurement Points and the Acquired Satellite Images Used in This Study

Research Area	St. ID	Lon.	Lat.	Acquisition Time		
				In situ (LT)	GOCI	Date
Mokpo Coastal Area (marked "B" in Fig. 1)	B10	126.07	34.97	9:10	UTC-00	Oct. 16th, 2012
	B09	126.03	34.97	9:28	UTC-00	
	B08	125.98	34.97	9:47	UTC-00	
	B07	125.94	34.96	10:04	UTC-01	
	B06	125.89	34.96	10:24	UTC-01	
	B05	125.85	34.96	10:40	UTC-01	
	B04	125.81	34.96	11:02	UTC-02	
	B03	125.72	34.96	11:40	UTC-02	
	B02	125.63	34.95	12:02	UTC-03	
	B01	125.54	34.95	12:31	UTC-03	
	A01	125.54	35.02	13:27	UTC-04	
	A02	125.63	35.03	13:54	UTC-04	
	A03	125.71	35.03	14:21	UTC-05	
	A04	125.80	35.03	14:48	UTC-05	
Gyeonggi Bay Area (marked "C" in Fig. 1)	C02	126.37	37.04	9:28	UTC-00	Jun. 11th, 2011
	C03	126.33	37.02	9:56	UTC-00	
	C04	126.29	37.01	10:20	UTC-01	
	C05	126.25	36.97	10:47	UTC-01	
	C06	126.22	36.93	11:13	UTC-02	
	C07	126.17	36.90	11:40	UTC-02	
	D10	126.13	36.93	12:02	UTC-03	
	D09	126.12	36.98	12:26	UTC-03	
	D08	126.17	37.00	13:10	UTC-04	
	D07	126.21	37.01	13:30	UTC-04	
	D06	126.25	37.03	13:52	UTC-04	
	D05	126.29	37.05	14:15	UTC-05	
	D04	126.33	37.07	14:38	UTC-05	
	D03	126.38	37.07	14:59	UTC-05	
	D02	126.41	37.07	15:19	UTC-06	
	D01	126.46	37.07	15:40	UTC-06	
	C01	126.47	37.05	15:55	UTC-06	

An in situ campaign in the Mokpo coastal area was performed on 16 October 2012. The measurement points, a total of 14 points, were along two separate lines (named A and B), as shown in Fig. 1(b). Among the points, the discrete distance was 8 km from A1(B1) to A4(B4) and 4 km from B4 to B10. In a similar in situ campaign in Gyeonggi Bay, we measured a total of 17 stations [7 C points and 10 D points in Fig. 1(c)] on 11 June 2011. These locations were determined to cover both the relatively clear water and the turbid water in the near-coastal area, an area that is dynamically changed in terms of ocean color even in a simple RGB image. Optical measurement data at the in situ sampling stations were obtained as types of downward irradiance ($E_d(\lambda)$), total upwelling radiance ($L_{wT}(\lambda)$), and sky radiance ($L_{sky}(\lambda)$) by using a FieldSpec 3 spectrometer by Analytical Spectral Devices (ASD) Inc. (hereafter ASD), which was able to measure spectral radiance and reflectance with a 1-nm interval and a spectral range of 350–1050 nm. To minimize environmental measurement error, such as direct sun glint and ship shadow, we controlled the ASD viewing angle and followed with

Mobley's measurement method [29]. These acquired optical properties of the sea surface were estimated and converted into nL_w values. The data used and matched between the GOCI and in situ measurement were a total of 14 positions and 6 GOCI images at times from UTC 00 to UTC 05, as listed in Table 1.

2.2. MTF estimation and compensation methods

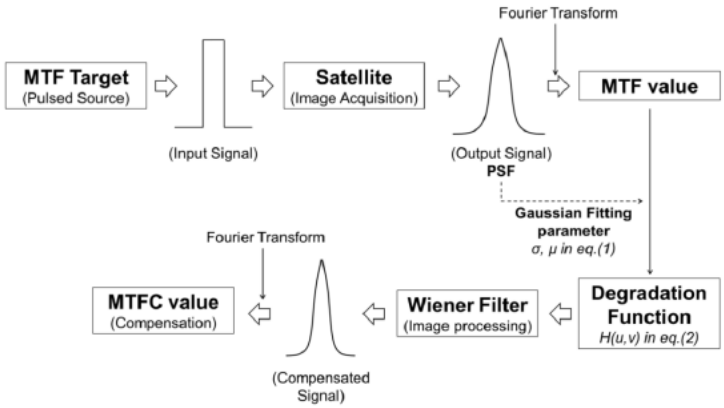

Fig. 2. Conceptual architecture of the MTF estimation process using the pulse method.

The MTF estimation process used in this report is based on the acquired image and a natural target serving as a pulse source. The pulse-source method used in this paper is widely applied for high-resolution satellites because it has the advantage of directly converting from a pulse source to a PSF value [13, 30]. Its method follows the estimating process shown in Fig. 2. First, when a satellite acquires an image, an input signal is blurred according to optical performance, including environmental effects [11]. As shown in Fig. 2, the blurring of a rectangular-shaped input pulse is changed to a curve-shaped PSF. The pulse width is determined by the geometric spatial resolution of the satellite and the size of the target area. The PSF value is then Fourier-transformed to an MTF value. However, in this conversion step, because noise is included in the pulse signal, the PSF shape lacks coherence, which can result in a calculation error, so a curve-fitting model should be applied to reconstruct the PSF. The Gaussian function that we used in this study is widely used for PSF fitting of high-resolution images, and it has the efficient advantage of fitting the curve with only two parameters, thus easily maintaining the high accuracy [13, 30, 31]:

$$g(x) = \frac{1}{\sigma\sqrt{2\pi}} e^{-\frac{1}{2}\left(\frac{x-\mu}{\sigma}\right)^2} \quad (1)$$

where σ and μ are the standard deviation and median value of the Gaussian curve, respectively. This standard deviation (σ) for Gaussian curve fitting is used in the principal values in the deconvolution process based on the WF.

The purpose of image restoration using MTF compensation is to remove noise from remote-sensing images and recover the original image. Fundamentally, the MTF compensation always has a reverse relationship between the amounts of noise and sharpening, so finding the optimal degradation model is a crucial issue. Thus, the existing MTF compensation method usually controls a regularization parameter as a constraint to produce a

#220807 - $15.00 USD Received 27 Aug 2014; revised 28 Sep 2014; accepted 11 Oct 2014; published 22 Oct 2014

3 November 2014 | Vol. 22, No. 22 | DOI:10.1364/OE.22.026908 | OPTICS EXPRESS 26913

stable deconvolution filter. In this paper, we selected the WF, which is one of the most widely used deconvolution filters and facilitates control of the degradation function [32, 33]. The computational process for the WF used in this paper is given in Eq. (2) as follows:

$$W(u,v) = \frac{H^*(u,v)}{|H(u,v)|^2 + \frac{S_n(u,v)}{S_f(u,v)}} = \frac{1}{H(u,v)} \cdot \frac{|H(u,v)|^2}{|H(u,v)|^2 + \frac{1}{SNR}} \quad (2)$$

where $W(u,v)$ is the WF value in the Fourier domain, $H(u,v)$ is the degradation function, $S_n(u,v)/S_f(u,v)$ is the ratio of the power spectrum of the noise and the undistorted image to the object, and (u,v) is the position in the spatial frequency domain. Generally, $S_n(u,v)/S_f(u,v)$ can then be approximated by an inverse SNR [34]. We fit the Gaussian function constructed with σ and μ to the degradation function ($H(u,v)$), and σ is used as a control parameter to each MTF compensated image in Section 3. SNR values were calculated with the nearly homogenous area in each band image [7, 8]. A signal value in SNR means the ocean radiance measured from target, and a noise value is assumed as an associated random variability. A statistical RMS noise of 5 × 5 pixels in homogenous area was obtained using the image based ocean noise estimation [7, 8]. The used SNR value is summarized in Table 2.

3. Results

Table 2 shows the normalized water-leaving radiance (nL_w) relationship between the GOCI image after the atmospheric correction and in situ measurement. In Table 2, the column indicates data type including the original image and MTF compensated images, which are separated according to the Gaussian value (σ) as a control parameter of the WF. For all of the spectral bands, this table compares the root mean square error (RMSE) value and R^2 written by the value (in parentheses) of nL_w. In the original image results, the minimum RMSE value was 0.0009 ($W/m^2/um/sr$) at band 8, but other band results were over 0.0020 ($W/m^2/um/sr$). When applied with the WF, the R^2 results changed slightly with a controlled Gaussian value (σ). Until σ was 0.3, little difference in accuracy was observed in terms of the RMSE, but the R^2 value was mostly enhanced, except at bands 4, 5, and 6. However, when setting the σ value to more than 0.4, we noticed a drastic change in both the RMSE and R^2 value. In particular, the R^2 values representing the co-relationship of data accuracy in bands 1 and 2 decreased from 0.83 to 0.49 and from 0.91 to 0.65, respectively (Table 2). The nL_w results are generally well correlated through all bands. The accuracy in the original image results shows an RMSE value of 0.009–0.0032 ($W/m^2/um/sr$) with an R^2 value of 0.83–0.94. Comparing with the MTF compensated results, when σ was 0.4, the result in the RMSE value was almost the same, but the R^2 value was slightly lower in all bands.

Furthermore, Fig. 3(a) illustrates variation in the nL_w value with increasing PSF correction value σ. When σ is 0.5 and 0.6, RMSE values increased drastically at all bands, which means that an excessive compensation is able to bring an unintended image data deformation. On the other points of view in the in situ measurement points, five points are selected in the offing (B1) to coastal area (B9) in Fig. 1. Figure 3(b) shows the MTF compensation influence results at the different ocean environments. These RMSE value at each location was estimated by comparing nL_w at all GOCI bands with those of in situ data. The B5 point value shows the worst RMSE results and huge variation according to σ value because this position is a boundary area between clear and turbid water regions. In the relationship among the five positions, Fig. 3(b) also shows that no difference exists from the original image until σ is 0.4.

#220807 - $15.00 USD Received 27 Aug 2014; revised 28 Sep 2014; accepted 11 Oct 2014; published 22 Oct 2014

Table 2. Statistical Results of the RMSE and R^2 Values for All Spectral Bands Applied with Modified MUMM Atmospheric Correction

		Band 1 (412nm)	Band 2 (443nm)	Band 3 (490nm)	Band 4 (555nm)	Band 5 (660nm)	Band 6 (680nm)	Band 7 (745nm)	Band 8 (865nm)
SNR		1045.77	870.36	698.11	595.48	379.85	350.870	299.99	222.14
Original Image		0.0023 (0.83)	0.0020 (0.91)	0.0024 (0.93)	0.0026 (0.94)	0.0032 (0.91)	0.0025 (0.93)	0.0021 (0.82)	0.0009 (0.83)
MTFC Image (σ)	0.1	0.0023 (0.83)	0.0020 (0.91)	0.0024 (0.93)	0.0026 (0.94)	0.0032 (0.91)	0.0025 (0.93)	0.0021 (0.82)	0.0009 (0.83)
	0.2	0.0023 (0.83)	0.0020 (0.91)	0.0024 (0.93)	0.0026 (0.94)	0.0032 (0.91)	0.0025 (0.93)	0.0021 (0.82)	0.0009 (0.83)
	0.3	0.0023 (0.83)	0.0020 (0.91)	0.0024 (0.93)	0.0026 (0.94)	0.0033 (0.91)	0.0025 (0.93)	0.0021 (0.82)	0.0009 (0.84)
	0.4	0.0023 (0.81)	0.0021 (0.90)	0.0025 (0.92)	0.0027 (0.93)	0.0034 (0.90)	0.0026 (0.93)	0.0021 (0.81)	0.0009 (0.83)
	0.5	0.0027 (0.74)	0.0024 (0.85)	0.0028 (0.89)	0.0031 (0.91)	0.0038 (0.87)	0.0029 (0.91)	0.0021 (0.81)	0.001 (0.83)
	0.6	0.0039 (0.49)	0.0038 (0.65)	0.0042 (0.76)	0.0044 (0.82)	0.0052 (0.76)	0.0041 (0.82)	0.0027 (0.72)	0.0015 (0.74)

Note: upper value means root mean square error value, and below value in parentheses shows R^2 value. Unit of both values is $W/m^2/um/sr$.

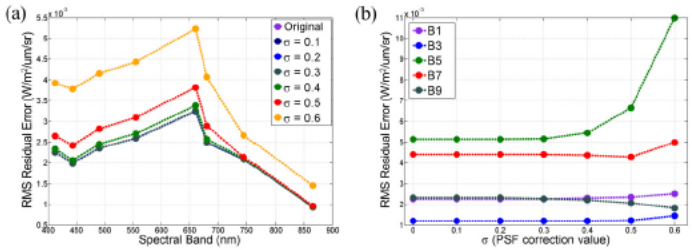

Fig. 3. (a) RMSE analysis between the MTF-compensated GOCI and in situ nL_w value for each band and the (b) relationship of the RMSE value at each in situ campaign position for the PSF correction value σ.

Figure 4 summarizes the MTF compensated target image from the improved MTF value and analyzes the interaction between the MTF value and derived nL_w accuracy via in situ measurements. MTF estimation is based on band-8 image which can show the best sharpness via other bands. The target seawall image series in Fig. 4(a) illustrates that three images (σ = 0.1–0.3) have similar pattern. However, the compensated parameter (σ = 0.4–0.6) causes the target image to be sharpened, and when σ is 0.5 and 0.6, a blurred image is generated around the target seawall image. This result can be interpreted to mean that each pixel value varies extremely due to the high compensation parameter σ. This shows that it is helpful to enhance the accuracy by increasing σ value, but extremely high σ values produce worse results, so the optimal compensation value is needed for remotely sensed image correction. According to the changing target image, Fig. 4(b) illustrates the increasing numerical trend of a compensated MTF value until reaching a σ value of 0.5, but the MTF value at the Nyquist frequency of the σ value of 0.6 (blue line) significantly decreased to 0.1154. Based on the calculated MTF value and the nL_w accuracy of the GOCI image, we could determine the optimal σ value from Fig. 4(b), which has the highest MTF value without influence of nL_w accuracy. When the MTF compensation parameter σ is 0.4, the Nyquist frequency MTF is 0.2152 at band 8, and

#220807 - $15.00 USD Received 27 Aug 2014; revised 28 Sep 2014; accepted 11 Oct 2014; published 22 Oct 2014

the RMSE value of the nL_w result is 0.0009 [Fig. 4(c)], which is the constant value of the original image result. The Nyquist frequency is defined as ½ of the sampling frequency, and in the case of GOCI, it is 33.8 mm^{-1} in the E–W direction and 43.4 mm^{-1} in the N–S direction.

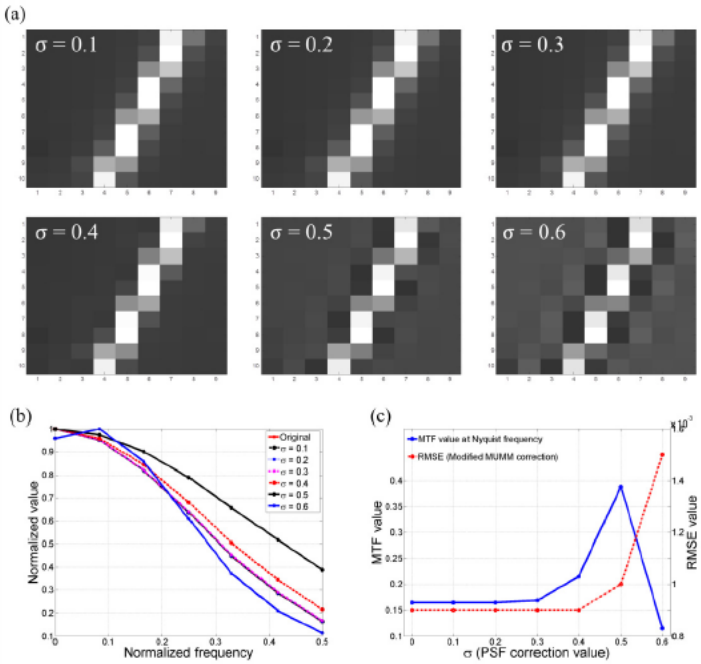

Fig. 4. Parametric analysis of the relationship between the MTF and accuracy of the ocean color product. (a) Target images of the Saemangeum seawall according to the PSF correction value σ, (b) MTF curve for the original image and six MTF-compensated images which is calculated from band-8 (865 nm), and (c) the relationship between the MTF value and RMSE according to the PSF correction value σ.

For verification of the optical compensated parameter, the MTF compensated image was generated with a σ value of 0.4. We compared two images in the Gyeonggi Bay area, as shown in Fig. 5(a). In the coastal area, we can distinguish the remotely sensed radiance change, and the compensated image has a higher degree of visibility in the entire target area. In particular, the water current can be well noticed, as shown in the enlarged image. In Fig. 5(a), for example, the waterway to the tidal flat (marked 'A') was represented in detail in the MTF compensated image compared with the original one. We could also clearly identify the boundary of a land part inside the tidal flat (marked 'B') in the MTF compensated image which had been blurred in the original image. In Fig. 5(b), the compensated MTF value is quantitatively enhanced in comparison to that of the original image, and the band-8 MTF value at the Nyquist frequency is changed from 0.1408 to 0.1871. This verification result shows the high correlation with the original nL_w value of the GOCI shown in Fig. 5(c). The RMSE and R^2 values between GOCI and MTF-compensated nL_w are 0.0001 and 0.9858, respectively. To summarize, these results mean that an MTF-compensated image with σ value

of 0.4 shows the enhanced sharpness and visibility without ocean product deformation of the original data.

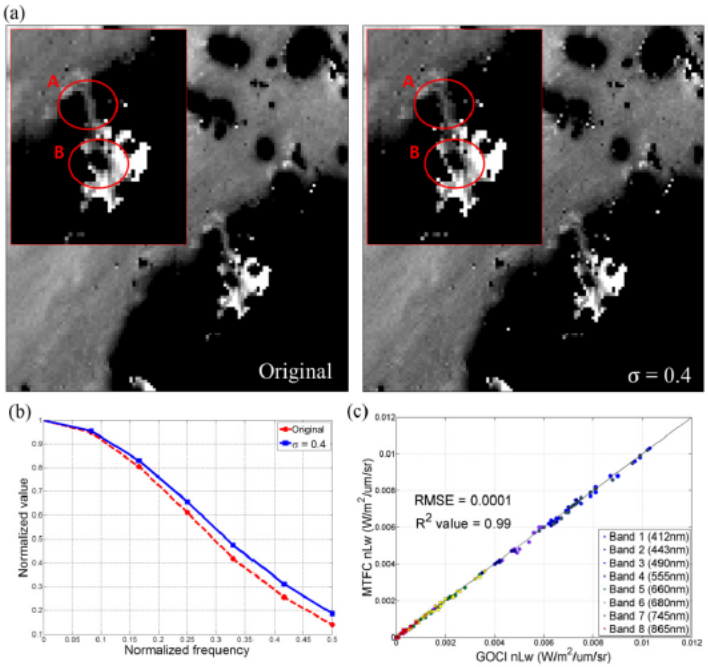

Fig. 5. Verification analysis with the estimated optimal compensation parameter (σ = 0.4) for the Gyeonggi Bay area. (a) Comparison results in band 6 between the original and compensated image, (b) MTF curve for the original image and MTF-compensated images, and (c) a correlation analysis between the GOCI and MTF-compensated image.

4. Conclusion

The goals of this study were to suggest the optimal parameter of MTF compensation by using the WF for GOCI images and to evaluate the co-relationship between the MTF value and the accuracy of the ocean color product (normalized water-leaving radiance, nLw). We calculated the in-orbit MTF value based on a pulsed natural target, and then applied the WF deconvolution to enhance the image quality of GOCI. In addition, to select the control parameter (σ) of the WF under minimum degradation of verification accuracy, we performed parametric case studies to compare GOCI images with in situ measured nL_w values. Then, we determined that the optimal σ value is 0.4, for which the MTF value at Nyquist frequency is enhanced to 0.2152 (original image: 0.1645) without the accuracy degradation of the ocean color product. Additionally, when we adjusted the same compensation parameter (σ = 0.4) to another target area and different image for verification, the enhanced image was similarly generated with a higher MTF value without deformation of the original data.

Conventionally, many scientists are concerned about pixel information damage of an image after MTF compensation. However, in this study, the suggested MTF-compensated model satisfies to generate sharpened images and to avoid the pixel information damage for

#220807 - $15.00 USD Received 27 Aug 2014; revised 28 Sep 2014; accepted 11 Oct 2014; published 22 Oct 2014

understanding ocean color phenomena. Especially, in case of the GOCI with a spatial resolution 500 m, it will be helpful to monitor the small-scale phenomena such as the water surface current near the coastal area and the narrow-pattern red tide stripe. One more advantage of using the MTF-compensated image is the ability to to differentiate cloud more accurately when applying atmospheric correction.

Acknowledgments

This research was a part of the project titled "Research for applications of Geostationary Ocean Color Imager(GOCI)" funded by the Ministry of Land, Transport and Maritime Affairs, Korea, and "Optical Performance Simulation of Geostationary Ocean Color Imager" of the Korean Institute of Ocean Science and Technology.

#220807 - $15.00 USD Received 27 Aug 2014; revised 28 Sep 2014; accepted 11 Oct 2014; published 22 Oct 2014

3 November 2014 | Vol. 22, No. 22 | DOI:10.1364/OE.22.026908 | OPTICS EXPRESS 26918

주 의

1. 이 보고서는 한국해양과학기술원 신진연구지원과제에서 수행한 연구결과보고서 입니다.

2. 이 보고서 내용을 발표할 때에는 반드시 한국해양과학기술원에서 수행한 연구결과임을 밝혀야 합니다.

3. 국가과학기술 기밀유지에 필요한 내용은 대외적으로 발표 또는 공개하여서는 안됩니다.